ADVANCED FUNCTIONAL MATERIALS
www.afm-journal.de

Machine Learning Enhanced Self-Charging Power Sources

Rui Gu, Liang Wei, Nuo Xu, Yao Xiong, Qijun Sun, and Zhong Lin Wang**

The widespread deployment of Internet of Things (IoT) networks has actualized omnipresent device interconnectivity. Despite technological advancements, IoT edge devices suffer persistent energy bottlenecks from suboptimal coordination of power acquisition and adaptive management. Self-charging power sources (SCPS) aim to achieve autonomous operation through monolithic integration of three core components: energy harvesters, power management circuits, and supercapacitors/batteries. These devices enable continuous ambient energy harvesting, providing uninterrupted power supply for wearable electronics and IoT applications. Nevertheless, material selection and component design remain key challenges in SCPS development. As an essential artificial intelligence paradigm, machine learning (ML) enables data-driven material and structural design based on historical experimental datasets, thereby elevating SCPS performance to superior level. This paper reviews the development of SCPSs and the application of ML in SCPSs, with a particular focus on SCPSs with triboelectric nanogenerators (TENGs) and supercapacitors (SCs). A generalized ML workflow with suggested parameters is proposed to guide the performance prediction of TENG by incorporating previous theoretical research. Additionally, ML-guided design of carbon-based SC materials and computer-aided suppression of self-discharge performance are selected as typical examples to discuss. The combination of ML and SCPS is expected to push forward more efficient and self-sufficient IoT applications.

1. Introduction

The rapid advancement of the Internet of Things (IoT)[1] and the ubiquity of wearable devices[2] have led to a proliferation of sensor networks distributed in various environments. These sensors, ranging from urban infrastructure to personal health monitoring applications, necessitate a reliable power supply for uninterrupted surveillance and data transmission. However, inherent limitations of batteries, such as restricted cycle life, protracted charging times, and environmental concerns arising from subsequent recycling, pose significant obstacles to the holistic development of the entire IoT system. Taking these factors into account, SCPS can harvest ambient energy and simultaneously charge energy-storage devices, offering a promising solution that can potentially eliminate the need for an external power source. SCPS represents an advanced technology dedicated to the collection, storage, management, and application of energy.

The concept of self-powered system and self-charging nanotechnology was first proposed by Prof. Wang in 2008,[3] emphasizing the integration of energy collection, storage, management, and application into a singular system to attain self-sufficiency. The inaugural study on a self-charging system was based on piezoelectric nanogenerators (PENGs). Subsequently, in 2010, Zhu et al.[4] designed a self-powered nanosystem that stored PENG energy into commercial capacitors through the utilization of a bridge rectifier. In 2011, Bae et al.[5] expanded upon the SCPS concept by integrating energy-harvesting PENG with supercapacitors, employing ZnO nanowires and graphene as foundational materials. Following the introduction of triboelectric nanogenerator (TENG),[6] SCPS based on TENG witnessed rapid advancement in various forms. For instance, Xiao et al.[7] have developed an SCPS utilizing fiber capacitors as energy storage devices, with TENG serving as the energy harvesting device.

SCPSs integrate critical components of energy harvesting, power management, and efficient energy storage, enabling them to provide uninterrupted power supply for wearable electronics and IoT applications instead of additional battery replacement.[8,9] The system's core elements are the energy-harvesting components and the energy-storage units. Numerous energy-harvesting devices have been investigated in SCPS studies, including solar cells,[10] TENG,[11] thermoelectric generators (TEG),[12] and PENG.[13] These technologies have their own distinct advantages and adaptability. Solar cells operate through solid-state photon-to-electron conversion, where semiconductor junctions generate electron-hole pairs upon absorbing photon energy. This mechanism achieves benchmark power conversion

L. Wei, N. Xu, Y. Xiong, Q. Sun, Z. L. Wang
Beijing Institute of Nanoenergy and Nanosystems
Chinese Academy of Sciences
Beijing 101400, China
E-mail: sunqijun@binn.cas.cn; zhong.wang@mse.gatech.edu
R. Gu, Q. Sun
School of Nanoscience and Technology
University of Chinese Academy of Sciences
Beijing 100049, China
L. Wei, N. Xu, Q. Sun
Center on Nanoenergy Research
School of Physical Science and Technology
Guangxi University
Nanning 530004, China
Q. Sun
Shandong Zhongke Naneng Energy Technology Co., Ltd
Dongying 257061, China

The ORCID identification number(s) for the author(s) of this article can be found under https://doi.org/10.1002/adfm.202505719

DOI: 10.1002/adfm.202505719

efficiencies that significantly surpass those of mechanical-to-electrical conversion systems and thermal gradient harvesters. For instance, the efficiency of the double-junction tandem solar cell developed by Liu et al. has reached 33.89%,[14] surpassing the single-junction Shockley–Queisser limit of 33.7% for the first time. TEG works based on the Seebeck or the Soret effect, where thermoelectric materials generate voltage in response to temperature gradients. The advantage of TEG lies in the absence of internal moving parts, long service life, noiseless and stable operation. The dimensionless figure of merit (ZT) serves as the primary metric for assessing thermoelectric materials, with state-of-the-art materials attaining ZT values between 2 and 3.[15–17] PENG converts applied mechanical stress into electrical energy through the piezoelectric effect. When mechanical stress is applied to non-centrosymmetric piezoelectric materials, the stress induces a change in the direction of polarization, leading to the generation of a potential difference. This potential difference drives alternating current (AC) in the external circuit. TENG can also convert mechanical energy into electrical energy based on the triboelectric effect, which is the coupling of contact electrification and electrostatic induction. PENG and TENG both have the characteristics of multiple structural designs, strong environmental adaptability and robustness.[18] In addition, TENG also has a wide range of material options, low manufacturing costs, and more flexible structural designs. These advantages make it highly suitable for SCPS applications in IoT. Traditional chemical batteries and supercapacitors (SC) are frequently employed as energy storage modules in SCPS. Compared to traditional batteries, SC offers superior charge-discharge rates, extended cycle life, superior environmental stability, and enhanced safety. These benefits make SC more compatible with TENG in SCPS, particularly in situations that necessitate frequent charge–discharge or require the rapid delivery of substantial energy within a brief timeframe.

In the context of SCPS, the collaborative operation among multiple components involves diverse device principles and complex structural design. This complexity poses substantial challenges for enhancing the system's sustainability and energy conversion efficiency. Traditional research methodologies predominantly employ experimental approaches to address these challenges, but they often fall short in handling tasks associated with complexity and diversity due to their time-consuming and resources-intensive nature. Consequently, there is an imperative need for a more efficient and streamlined approach to expedite the development and enhancement of SCPS components and overall performance. Machine learning (ML) has emerged as a pivotal technology capable of aiding in the design of SCPS, offering cost reduction and enhanced system sustainability.

This work provides a systematic review on the most recent advancements in SCPS, specifically those based on TENG and SC. It also encapsulates the current status of ML-assisted design optimization for energy harvesting/storage devices, as depicted schematically in **Figure 1**. In light of the scarcity of research on ML-assisted TENG performance optimization, this paper summarizes a universally applicable ML workflow and some key parameters for TENG performance optimization that can serve as a reference for device design. The discussion concludes with a forecast of future prospects and challenges associated with the use of ML to assist in the design of SCPS.

2. Self-Charging Power Source

TENG has garnered significant interest from the scientific community due to their capacity to harvest a variety of previously overlooked mechanical energy resources from the surroundings.[19] The potential of TENG is remarkable, attributed to its high output, cost-effectiveness, and eco-friendly characteristics. Consequently, research on this technology has surged in recent years.[20] However, the output signal of TENG is an alternating current (AC), which cannot be directly stored like conventional energy-harvesting systems. It necessitates initial connection to a rectifier unit with a post-circuit management before being directed into a storage unit, thereby ensuring efficient energy utilization. A complete SCPS (**Figure 2a**) can provide continuous power supply to electronic devices. Typically, the energy storage devices for the TENG-based SCPS are primarily batteries and SCs. SCs have higher power density and better cycle stability compared to batteries. Therefore, this section primarily discusses the SCPS constructed using TENG and SC.

In light of the swift advancements in wearable electronics, traditional rigid self-charging devices have become inadequate for integration with flexible clothing. Consequently, a novel fiber-like self-charging system has been introduced. Yang et al.[21] propose a 1D coaxial fiber-like self-charging system that incorporates an external TENG and internal SC (Figure 2b). This configuration not only harnesses energy through the external TENG, but also stores it within the inner fibrous SC, thereby achieving both mechanical energy harvesting and storage. Within this design, carbon fiber is employed as the electrode material for the TENG and SC. Concurrently, silicone rubber functions as both a separator and a triboelectric layer. Both the SC and TENG demonstrate remarkable stability, ensuring prolonged durability for everyday use. Han et al.[22] have developed a coaxial energy yarn tailored for multifunctional applications of energy harvesting/storage/utilization. The fiber-like TENG boasts a peak output power of 2.5 μW, while the fiber-like SC exhibits a specific capacitance of 13.42 mF cm^{-1}. Furthermore, the fiber-like self-powered tactile sensor demonstrates a sensitivity of 1.003 V kPa^{-1}. Beyond its utility in powering wristwatches and thermometers, this energy fiber is also capable of performing functions such as pressure sensing and smart identification.

Individual fibers generally possess limited mechanical strength and load-bearing capacity. To enhance the performance, researchers have woven fibers into some textiles or directly incorporated fibers into fabrics to establish a textile self-charging system. Hu et al.[23] have developed a self-charging functional textile comprising a yarn-based TENG and a yarn-based asymmetric SC. The TENG yarn is integrated into the textiles' daily wear, thereby harnessing the biomechanical energy produced from human motions. With a short-circuit current of 2 μA for the fabric TENG and a areal energy density of ≈78.1 μWh cm^{-2} for the yarn-based SC, the combined textile SCPS can power a watch without an external power source. Dong et al.[24] have introduced a power textile knitted in an all-yarn structure that exhibits self-charging ability, high stretchability, and excellent washability even after multiple cycles (Figure 2c). This textile maintains high strength, elasticity, toughness, and good stretchability, accommodating the dynamic movements of the human body. By integrating the yarn-based TENG and yarn-based

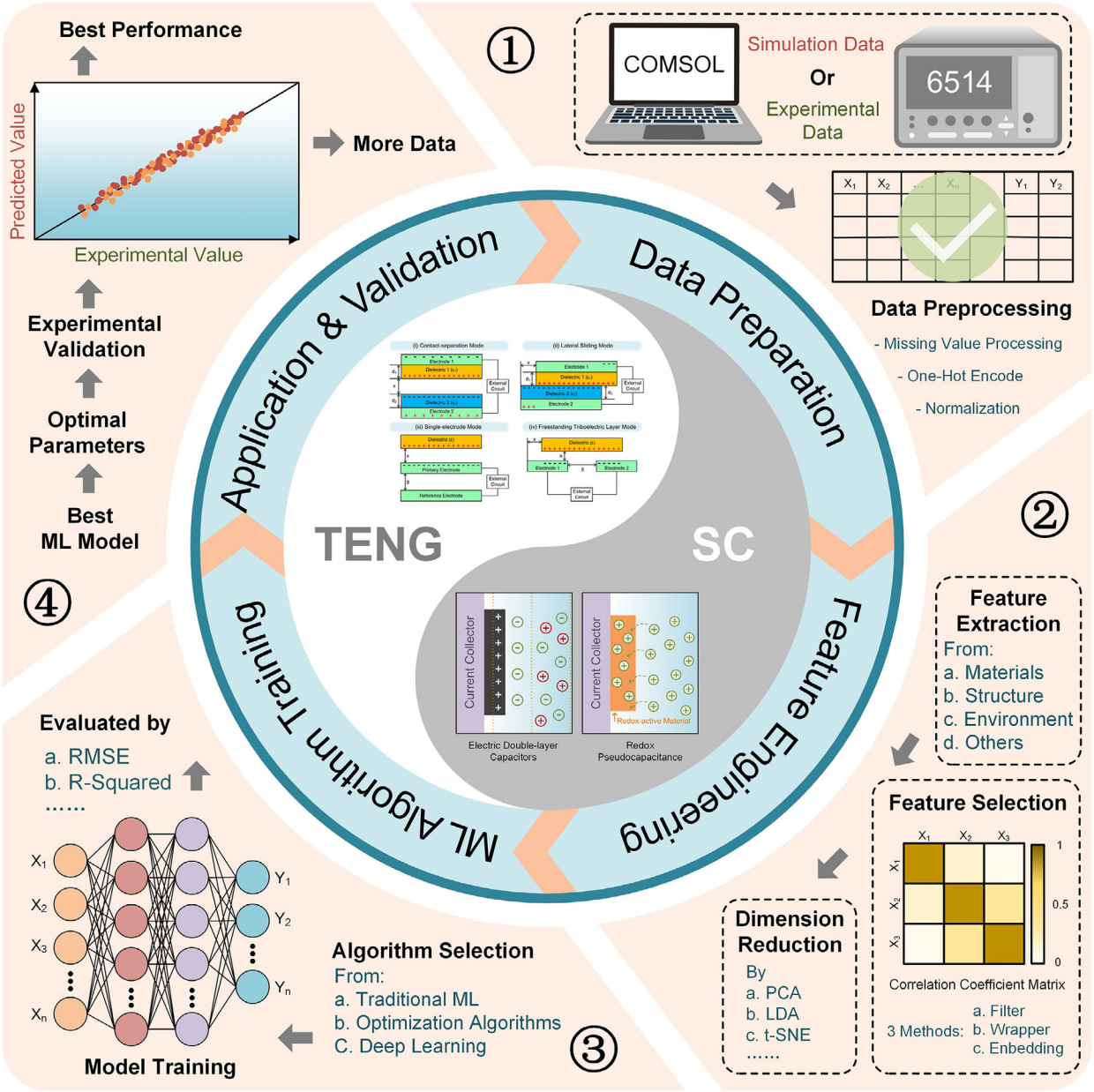

Figure 1. Machine learning enhanced self-charging power source based on TENG and SC.

SC through weft knitting, the resulting textile demonstrates superior elasticity, toughness, and stretchability. Pu et al.[25] have reported another self-charging power textile using yarn SC with reduced graphene oxide as the active material, achieving a capacitance of up to 13 mF cm^{-1}. The TENG rapidly supplies power to the SC (charging to 2.1 V within 2009 s), enabling it to power a watch without an external power source. Wang et al.[26] have described a specific self-charging power textile in a coplanar fashion by incorporating micro SC (MSC) with TENG fabricated via one-batch resist-dyeing method. The MSC exhibits a commendable maximum areal capacitance (50.6 mF cm^{-2}), while the fabric TENG boasts an outstanding peak power density (94.5 mW m^{-2}). The fabric-based SCPS holds promising prospects for future development and application in wearable electronics.

The trend in flexible electronic devices is toward being lightweight and thin, leading to the rapid development of SCPSs that meet the same requirement. Sun et al.[27] have proposed a self-supplying functional paper-based device, comprising an all-paper TENG, a power management system, a SC, and a back-end application circuit (Figure 2d). Each module operates independently but integrates to form the complete functional paper-based device. The paper-based TENG can readily charge a 2.2 μF commercial capacitor to 10 V in 19 s. The paper-SC also attains a maximum areal specific capacitance of 1.6 mF cm^{-2} under a discharging current density of 2 μA cm^{-1} in galvanostatic

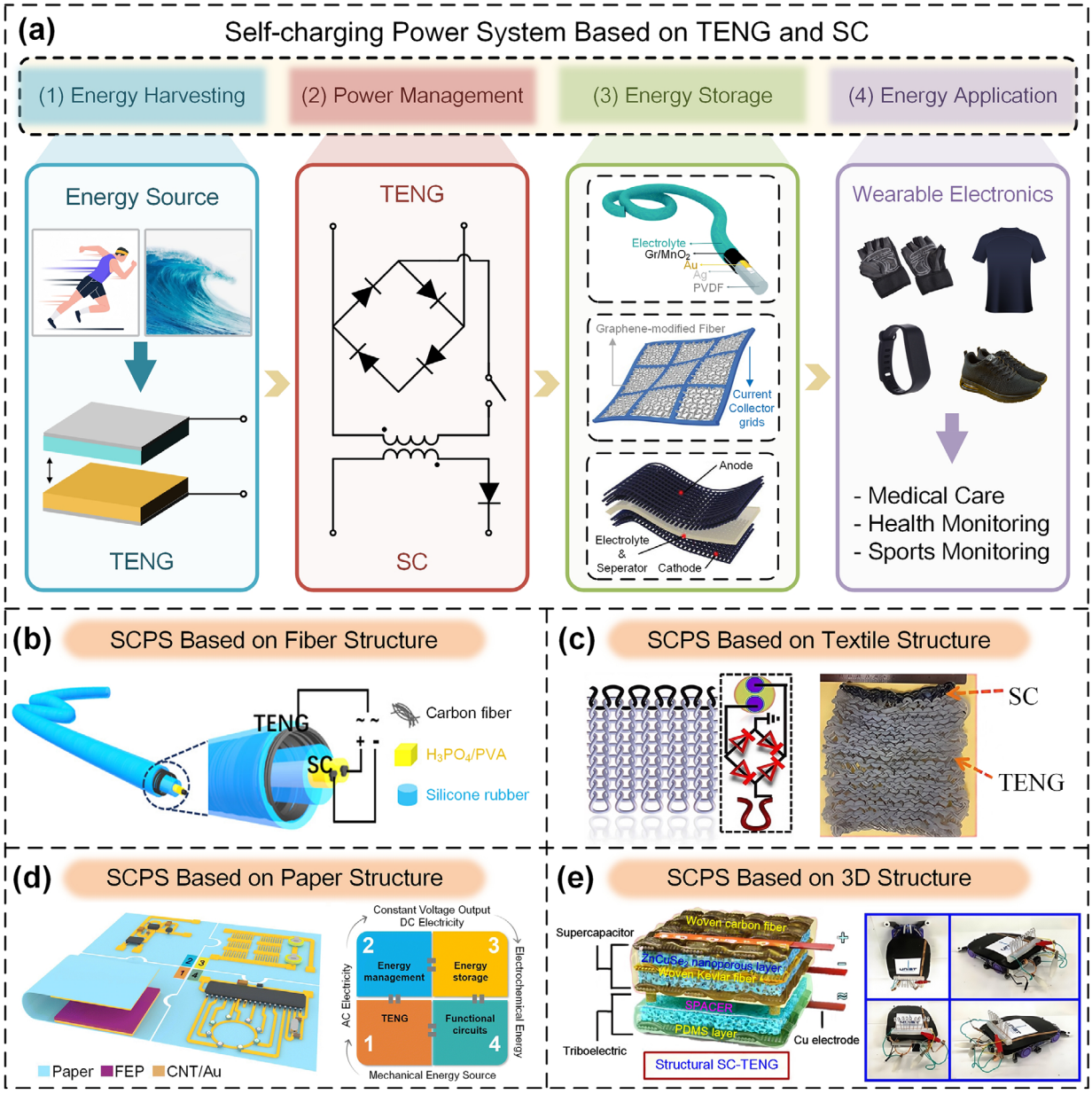

Figure 2. a) Schematic diagram of self-charging power system based on TENG and SC. Top of energy storage section: Reproduced with permission.[167] Copyright 2021, Royal Society of Chemistry. The middle part of energy storage section: Reproduced with permission.[168] Copyright 2016, Wiley-VCH. Bottom of energy storage section: Reproduced with permission.[169] Copyright 2021, Wiley-VCH. b) Fabric-based self-charging device structure and circuit. Reproduced with permission.[21] Copyright 2018, American Chemical Society. c) Textile-based self-charging device structure, circuit, and actual photo. Reproduced with permission.[24] Copyright 2017, American Chemical Society. d) Planar paper-based structure, schematic of multifunctional module. Reproduced with permission.[27] Copyright 2022, Royal Society of Chemistry. e) Integrated self-charging energy pack structure, circuit, physical demonstration. Reproduced with permission.[29] Copyright 2021, Elsevier.

charge–discharge (GCD) tests. The paper-based PMC module has a power management efficiency of up to 53.6%, with power supply applications including light-emitting diodes (LEDs), temperature/humidity sensors, and an infrared wireless transmitter. The demonstrated self-powered functional paper module introduces a pioneering paradigm for sustainable functionality and multifunctional circuits. Song et al. have demonstrated an environmentally friendly self-charging system based on paper.[28] A layer of gold is sputtered on the surface of commercial paper through shadow mask, serving as an electrode for both the TENG and MSC. This paper-based self-charging model has the potential to power global positioning system devices. Furthermore, the active electrode material of MSC can be directly written by a pencil and amenable to surface functionalization to significantly increase energy storage capacity while reducing production costs.

In addition to fibers, fabrics, and planar structures, more diverse structural designs have been explored on integrated self-charging energy packages. Deka et al.[29] have reported a

self-charging energy packet (Figure 2e). The power of the TENG based on woven carbon fiber (WCF) has reached up to 8.9 mW, while the energy density of the WCF-based SC can reach up to 1.93 Wh kg^{-1}. The specific surface of the WCF could be significantly enhanced by coating the N-doped Zn-Cu selenide nanoporous material onto the WCF surface, thereby improving the energy storage capacity of the SC. Concurrently, this structure exhibits excellent mechanical strength of 453.97 MPa and modulus of 35.29 GPa, making it highly suitable for future automotive and aerospace applications. Qin et al.[30] have demonstrated an intelligent self-charging energy package capable of determining the charging state with an electrochromic SC through its color change. The integrated SC array can be self-charged to 3 V, subsequently illuminating the LEDs. This straightforward and cost-effective method of smart self-charging power packs holds potential for future daily electronics applications. Li et al.[31] propose a new method for fabricating integrated energy conversion and energy storage devices by combining TENG and capacitors based on poly(vinylidene fluoride)-*co*-hexafluoropropylene. The device significantly enhances TENG performance, achieves stable DC voltage, and is capable of powering a digital calculator and laser diode. It also performs excellently even in a miniaturized size of 1 × 1 cm, with a maximum output voltage of 271 V. This work provides a novel strategy to develop high-performance SCPS.

3. ML for Energy Harvesting and Storage

ML represents a significant branch of artificial intelligence. Recently, it has made substantial advancements in aiding the development of new materials and the design of specialized devices.[32–35] In the realm of material and device optimization, the utilization of ML can significantly expedite the process of material discovery and structural optimization. Conventional material research requires extensive experimental resources and prolonged development cycles, whereas ML technology enables accelerated process optimization. Through ML technologies, researchers can refine models by learning from existing datasets. Subsequently, these optimized models can be used for prediction and simulation to guide experimental design and material development. For SCPS, ML offers significant potential to optimize individual components, particularly energy harvesting/storage devices, thereby enhancing the efficiency and performance of the whole system. This section will discuss the basic types of ML and its important applications in energy harvesting and storage devices.

ML can be categorized into three primary learning methods: supervised, unsupervised, and reinforcement learning. Thereinto, supervised learning involves training algorithms to optimize predictive models using labeled datasets, enabling accurate predictions on new data. This method is typically employed for classification and regression problems, with the optimization of novel energy materials or devices largely reliant on this approach. In contrast, unsupervised learning analyzes unlabeled datasets through techniques such as clustering, dimensionality reduction, and association rule mining. Reinforcement learning constitutes a decision-centric paradigm where algorithms iteratively interact with environments through trial-and-error mechanisms, dynamically adjusting strategies to maximize cumulative reward.

The selection of algorithms is fundamental to ML technology, serving as a tool for extracting information from data, discerning patterns, and making informed decisions. As illustrated in **Figure 3**, this paper primarily explores the application of ML in energy-storage materials and energy-harvesting devices. Related research involves a variety of ML models, such as linear regression (LR), decision trees (DT), random forests (RF), and support vector machines (SVM), as well as artificial neural networks (ANNs), including deep neural networks (DNNs), convolutional neural networks (CNNs), recurrent neural networks, graph neural networks (GNNs), among others. These ML algorithms have found extensive applications in energy harvesting, specifically in materials and devices based on photovoltaic,[36–43] thermoelectric,[44–51] piezoelectric,[52–55] and triboelectric technologies.[56–60] Additionally, they have been extensively utilized in energy storage, particularly in batteries and SCs.

Traditional ML algorithms demonstrate optimal performance with structured datasets and limited-scale applications, typically requiring manual feature engineering. Hu et al.[38] explored the performance and key influencing factors of perovskite solar cells using multiple regression algorithms. They trained the optimal model using SVM algorithm and subsequently designed a long-term ambient stable perovskite solar cell with an energy conversion efficiency of 23.4%. Karade et al.[40] have employed various algorithms to predict the optimal manufacturing conditions and device parameters of $Cu_2ZnSn(S,Se)_4$ thin film solar cells. Based on optimized DT and classification and regression tree rules, in conjunction with a well-trained RF model, they have achieved the highest average power conversion efficiency (PCE) of over 10.1% (champion device ≈11.0%). Jing et al.[53] have utilized six ML algorithms, namely least absolute shrinkage and selection operator (LASSO), AdaBoost regressor, support vector regressor (SVR), random forest regressor, extreme gradient boosting regressor (XGBoost), and gradient boosting regressor (GBR), to predict the performance of aluminum nitride-based piezoelectric materials with varying concentrations and compositions. The GBR model outperformed the others in terms of performance, with a mean absolute error (MAE) of 0.21 and R-squared (R^2) of 0.79. Saeidi Javash et al.[48] have pioneered the integration of ultrafast flash sintering with Gaussian process regression ML models and Bayesian optimization to predict the optimal flash sintering variables for n-type silver selenide thermoelectric films. This approach ultimately aided in designing flexible thermoelectric film with a ZT value of 1.1.

Deep learning offers a robust solution for addressing unstructured data and large-scale problems. This methodology employs multilayer neural networks that autonomously learn hierarchical feature representations, significantly reducing dependence on manual feature engineering. Wang et al.[42] leveraged ML to develop an exceptional model for predicting the PCE of organic solar cells, achieving a correlation coefficient (r) of 0.79. They have implemented efficiency models based on molecular properties and property models that establish the relationships between properties and molecular structures using the light gradient boosting machine algorithm and GNN algorithm, respectively. Li et al.[50] implemented a neural network-based transfer learning (TL) strategy for electron bandgap prediction, demonstrating high accuracy in forecasting ZT values of

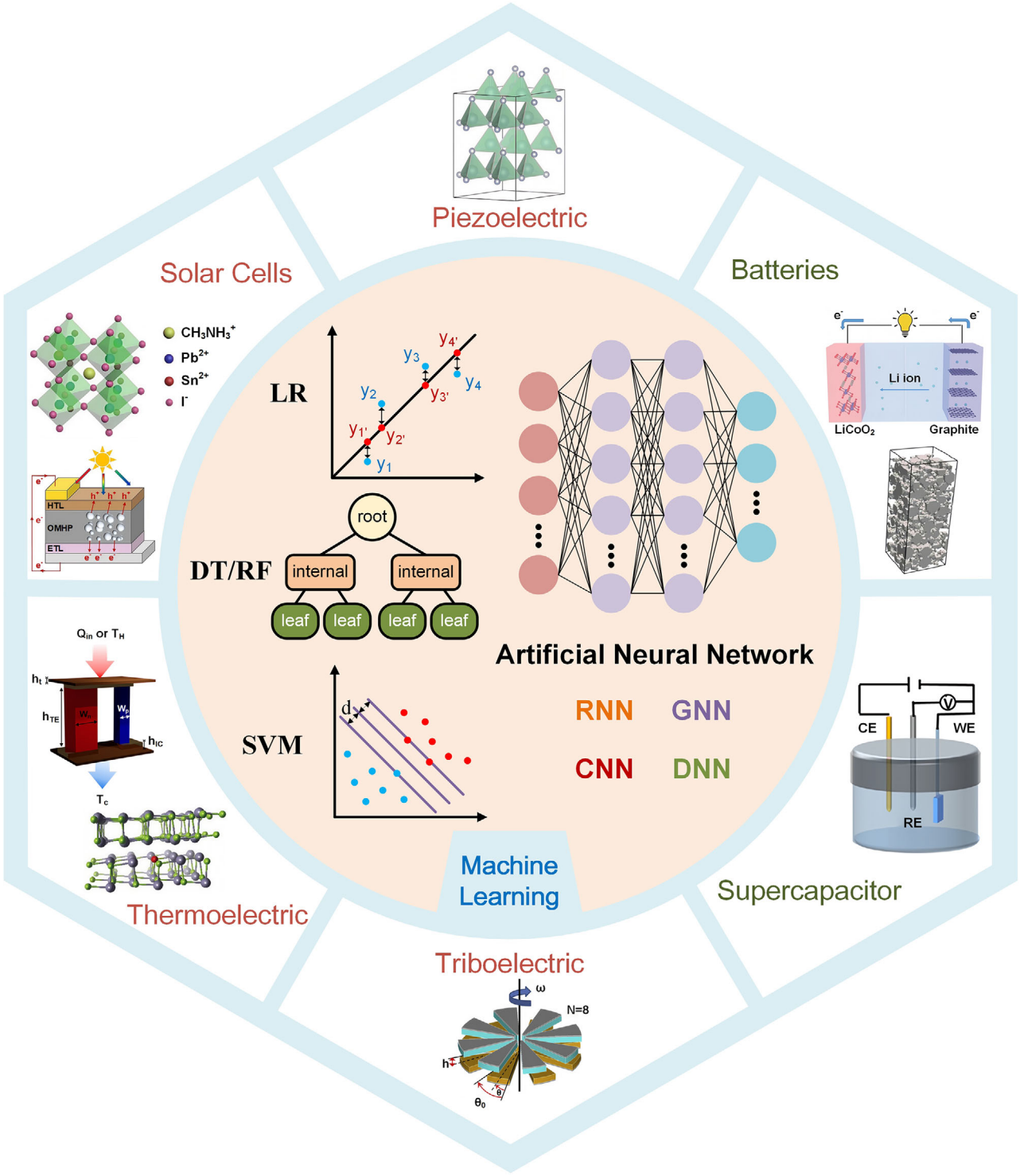

Figure 3. The application of ML in energy harvesting and storage. The inner circle displays examples of several commonly used ML algorithms. The hexagonal outer ring showcases technologies related to various energy harvesting devices and energy storage devices. Piezoelectric device: Reproduced with permission.[53] Copyright 2023, Royal Society of Chemistry. Solar cells: Reproduced with permission.[43] Copyright 2022, The Authors. Thermoelectric device: Reproduced with permission.[44] Copyright 2021, Elsevier. Thermoelectric material: Reproduced with permission.[45] Copyright 2022, American Chemical Society. Triboelectric nanogenerator: Reproduced with permission.[56] Copyright 2020, Elsevier. Lithium battery: Reproduced with permission.[138] Copyright 2021, Wiley-VCH. Electrode material: Reproduced with permission.[170] Copyright 2023, The Authors. Supercapacitors: Reproduced with permission.[171] Copyright 2023, The Authors.

thermoelectric materials at any given temperature. When compared to direct ML, the TL model increased the Pearson correlation coefficient of p-type systems from 23% to 95%, and the coefficient of n-type systems from 46% to 94%. Recently, Merchant et al. have proposed a large-scale active-learning ML model known as graph networks for materials exploration, which has achieved unprecedented efficiency in material discovery. This advancement holds significant implications for material discovery in areas such as batteries and photovoltaic technology. Zhu et al.[44] proposed a hybrid framework integrating genetic algorithm (GA) with ANN for power performance optimization. Their findings reveal that this combined methodology achieves negligible deviation from COMSOL multiphysics simulation results while accelerating parametric analysis by over three orders of magnitude compared to conventional finite-element approaches. This breakthrough demonstrates the potential of machine learning-enhanced computational strategies in overcoming the time-accuracy trade-off inherent in mechanoelectrical system design.

4. ML for TENG Performance Optimization

TENG is an important energy harvesting unit in SCPS, and using ML to improve TENG performance is an important step in system optimization. This section will provide a succinct overview on the fundamental mechanism and current advancements in TENG technology, followed by a review of the progress made in computer-aided optimization of TENG design. Lastly, we propose a generalized ML architecture along with suggested parameters to predict the output performance of TENG.

4.1. Triboelectric Nanogenerators

Since its introduction in 2012,[6] TENG has transitioned from a fundamental physical concept to an efficient technology for energy harvesting. The mechanical-electrical energy conversion in TENG primarily involves two processes: contact-electrification (CE) and electrostatic induction. While CE was first observed over 2600 years ago, there still remains no universally accepted unified scientific understanding of its mechanism. Research by Wang et al.[61,62] suggests that electron transfer is the primary mechanism governing interface charge processes in solids, liquids, or gases. Building on the dominant working mechanism of electron-emission assisted charge-transfer process, Xu et al.[63] have proposed an electron-cloud–potential-well model (**Figure 4a**), which can account for all types of CE based on conventional materials. In this model, atoms are depicted as potential wells, with electrons outside the shell loosely interacting to form an electron cloud for each atom or molecule. As illustrated in Figure 4a(i), d represents the distance between electron clouds, E_A and E_B denote the occupied energy levels of electrons in the atoms of two different materials A and B, and E_1 and E_2 represent the potential energy required for electrons to escape from the surfaces of material A and material B, respectively. Prior to the contact between the two materials, electrons are confined by the local trapping effect of their potential wells and cannot be transferred. Upon contact (Figure 4a(ii)), electron clouds from both materials overlap, forming an asymmetric double potential well that enables electrons to transition from atoms of material A to those of material B. When separated (Figure 4a(iii)), the energy barrier E_2 in material B retains most of the transferred electrons if the temperature is not excessively high. This process corresponds to the CE phenomenon occurring between electropositive material A and electronegative material B. Figure 4a(iv) illustrates that an increase in temperature T corresponds to a proportional rise in electron energy, as indicated by the growth of $k{\cdot}T$. This trend facilitates the transition of electrons from the potential well. The proposed electron-cloud–potential-well theory provides a comprehensive understanding on the CE behavior across various material types.

The design of a TENG necessitates both structural innovation and the optimization of multiple materials,[64–71] which can help to optimize its energy collection efficiency and to accommodate varying application requirements. As illustrated in Figure 4b, the prevalent working modes of TENG encompass contact-separation, lateral sliding, single-electrode, and freestanding working modes, respectively. Taking the contact-separation mode TENG as an example, when two distinct materials come into contact, the disparity in electron affinity between them results in materials with higher electronegativity acquiring electrons from those with lower electronegativity. This process generates opposing charges on the contact surface of the two materials. Following this, when these materials are separated, the potential difference between each other creates an electric field. This electric field drives electrons to flow from one material to another via an external circuit, thereby generating an output current. In subsequent cycles, the repeated contact-separation process continuously generates alternating current, facilitating the mechanical-electrical energy conversion.

Compared to conventional energy-harvesting technologies, TENG exhibits several advantageous characteristics,[11] encompassing cost-efficient production, simple fabrication processes, robust low-frequency energy harvesting capabilities, strong environmental adaptability, broad material compatibility, and self-powered functionality. These attributes have established TENG as a transformative technology for energy harvesting and self-powered sensing applications. Not only can TENG harness energy from human movement,[72] but it can also collect environmental energy from vibrations,[73] wind,[74] raindrops,[75] and waves[76] present in the environment. Remarkably, TENG can gather this environmental energy with no requirement for external power source, which can then be utilized to power sensors and enable energy-autonomous operation. This type of sensor holds significant potential for application across various fields such as smart homes,[77] health/motion monitoring,[78,79] biomedicine,[80] smart transportation,[81] robotic systems,[82] environmental monitoring,[83] etc.

4.2. Computer-Aided TENG Optimization

Current research integrating TENG with ML techniques predominantly focuses on sensing applications. These studies utilize ML to analyze the signals gathered from TENG sensors, aiming to enhance signal processing efficiency and accuracy. This approach empowers TENG sensors not only to effectively convert mechanical energy to electrical energy but also to execute more intricate

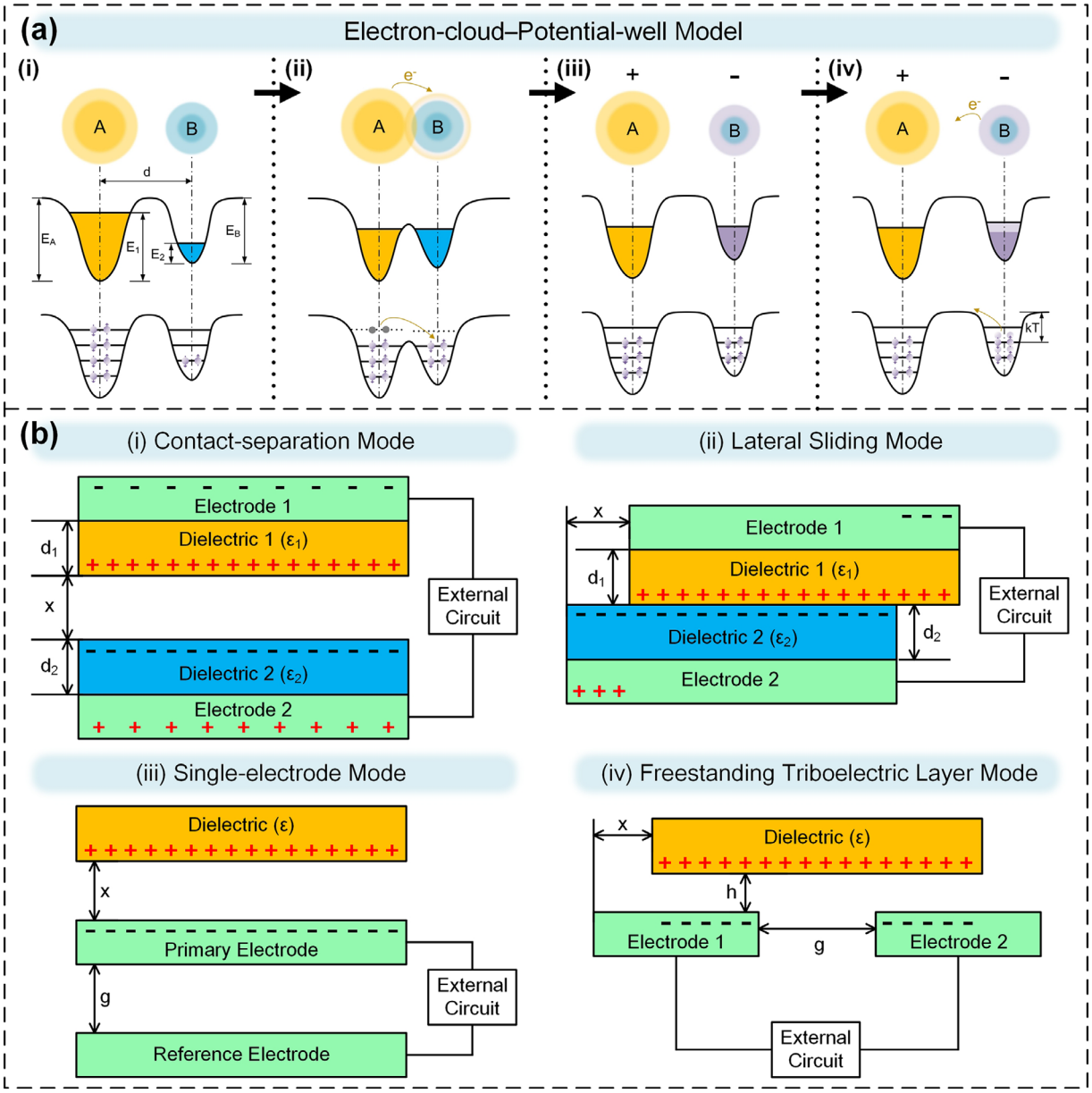

Figure 4. The common principle and working modes of TENG. a) Electron-cloud–Potential-well Model. b) The four common working modes of TENG.

tasks such as action recognition, health monitoring, and environmental surveillance through intelligent data analysis. While ML has been extensively applied to TENG sensors, its systematic research for device design and material optimization remains nascent.

Table 1 Summarize recent studies on the influence of structural parameters (e.g., grating number, grating space, grating width) on the output performance of TENG devices. Khorsand et al.[56] have tried to integrate the mathematical model of rotating TENG with the grey wolf optimization (GWO) algorithm, analyzed the relying of generated energy on kinematic/geometric parameters, and derived the optimal distribution of transferred charges, output voltage/current, and harvested mechanical energy. Wang et al.[57] have employed SVR algorithm to process finite element simulation data of cyclic graphing structured TENG to achieve higher accuracy fitting results. By integrating SVR with numerical analysis, specially the Runge–Kutta method, the structural parameter *n* of TENG was effectively optimized. This study also analyzed the impact of key parameters, such as the gap *h* between the rotor and the stator and the partial capacity on TENG performance across varying values of *n*. Jiang et al.[58] employed a stochastic gradient descent (SGD) to optimize a DNN model based on experimental data, predicting the output performance of three distinct TENG types: graded structure, disc structure, and rolling structure. This approach offers a novel strategy for optimizing TENG performance. Zhou et al.[59] performed finite element analysis and equivalent circuit simulation using COMSOL Multiphysics and MATLAB Simulink, respectively. They

Table 1. Research on optimizing TENG performance with AI/ML algorithms.

Date	TENG structure	ML algorithms	Key parameters
2020[56]	Rotary	GWO	Grating space, angular velocity, tribo-spacing, etc.
2021[57]	Cylindrical grating-structured	SVR	Grating numbers, stator gap, parasitic capacitance, etc.
2022[58]	Grating, disc, and rolling	SGD, DNN	Grating width, sliding velocity, gap distance, etc.
2023[59]	Rotary	NSGA-II	Outer radius, electrode pairs, and electrode gap

subsequently applied a non-dominated sorting genetic algorithm II (NSGA-II) to the resulting data to derive an optimized free-standing rotational TENG performance model.

In addition to studying the impact of structural parameters on TENG device performance, ML technology also plays an important role in key material discovery. Zhang et al.[84] applied the backpropagation neural network of differential evolution algorithm to determine the electrical properties of flexible Ag/poly (amic acid) (PAA) composite structures. The study used PAA concentration, ion exchange time of $AgNO_3$, concentration and reduction time of $NaBH_4$ as characteristic parameters, and the product of thin layer resistance and treatment time of Ag/PAA thin films as the target parameter to establish a high-precision ML model with a relative prediction error of less than 1.96%. Hu et al.[85] used SVR models to predict the dielectric constant and bandgap of binary and ternary oxides. The determination coefficient R^2 of the final model in predicting the dielectric constant is 0.886, and the root mean square error (RMSE) is 0.083; In bandgap prediction, R^2 is 0.832 and RMSE is 0.533. The model significantly improves computational efficiency and prediction accuracy compared to traditional methods. In addition, the mechanical properties of the triboelectric layer material also have an impact on the durability and stability of TENG devices. Wang et al.[86] studied the tribological properties of polytetrafluoroethylene (PTFE) composite materials by combining experimental analysis with ML. It was found that the friction coefficient and wear rate of PTFE composite materials decrease with increasing speed, while an increase in temperature leads to an increase in wear rate and a decrease in interfacial bonding strength. The GBR model performs the best in predicting wear rate ($R^2 = 0.91$, RMSE = 4.34), and Pearson correlation coefficient indicates that speed and temperature are the most significant factors affecting friction coefficient and wear rate.

4.3. Selection of Features and Targets

The selection of targets in research typically hinges on the specific objectives of the study. Open-circuit voltage (V_{OC}), short-circuit current (I_{SC}), and transferred charge (Q_{SC}) are commonly chosen as the algorithmic targets due to their straightforward measurement, which facilitates the characterization of TENG performance. Depending on the research objective, additional parameters such as energy conversion efficiency, output power, and cycle stability can also be selected as targets.

Regardless of the ML algorithm employed, the selection of appropriate features takes into account multiple factors associated with TENG performance, including but not limited to its material properties, structural design parameters, operating conditions, and environmental impact factors. Drawing from previous theoretical studies on TENG, the selected features are categorized into three types in the proposed general model: structural parameters, material parameters, and environmental parameters. Using the neural network model as an illustrative example, the relationship between these features and targets is depicted in **Figure 5**a.

4.3.1. Structure Parameters

The structural parameters influencing TENG performance typically encompass the maximum displacement area X_{max}, device area A, dielectric layer thickness d and load resistance R. For ease of classification, this paper considers the maximum displacement distance X_{max} as a structural parameter, despite it not being an integral part of the TENG structure.

Zi et al.[87] introduced a universal benchmarking method for evaluating the performance of various TENGs in 2015. This method, termed performance figure-of-merits (FOM_P) of TENGs, comprises figure-of-merits for structural attributes (FOM_S) and figure-of-merits for materials (FOM_M), described by the formula as follows:

$$FOM_P = FOM_S \cdot FOM_M = \frac{2\varepsilon_0}{\sigma^2}\frac{E_m}{AX_{max}} \cdot \sigma^2 = 2\varepsilon_0 \frac{E_m}{AX_{max}} \quad (1)$$

In the given formula, ε_0 represents the vacuum dielectric constant, σ denotes the triboelectric surface charge density, E_m signifies the maximum energy achieved in a single working cycle, A denotes the device's area, and X_{max} indicates the maximum displacement area. As inferred from the referenced study, the ratio of E_m/AX_{max} is indicative of TENG properties, with A included in the denominator to mitigate the TENG volume influence on the output performance. Consequently, it can be deduced that the structural parameters influencing TENG performance encompass both the maximum displacement area X_{max} and device area A.

Shao et al.[88] have conducted a study in 2018 on the structural optimization of TENG taking into account the load resistances. For each of the four fundamental modes of TENG, they not only evaluated performance under varying load resistances R but also investigated the influence of X_{max} on the output performances. Liu et al.[89] developed a qualitative benchmark for evaluating the contact efficiency between electrodes and dielectrics in TENG. By implementing various parameter modifications, such as diminishing the dielectric thickness, augmenting external capacitors, modulating the atmospheric conditions, and optimizing surface contact levels, they achieved a high charge density. This study suggests that modifying the dielectric layer's thickness, dented as d, can markedly influence the output performance of TENG.

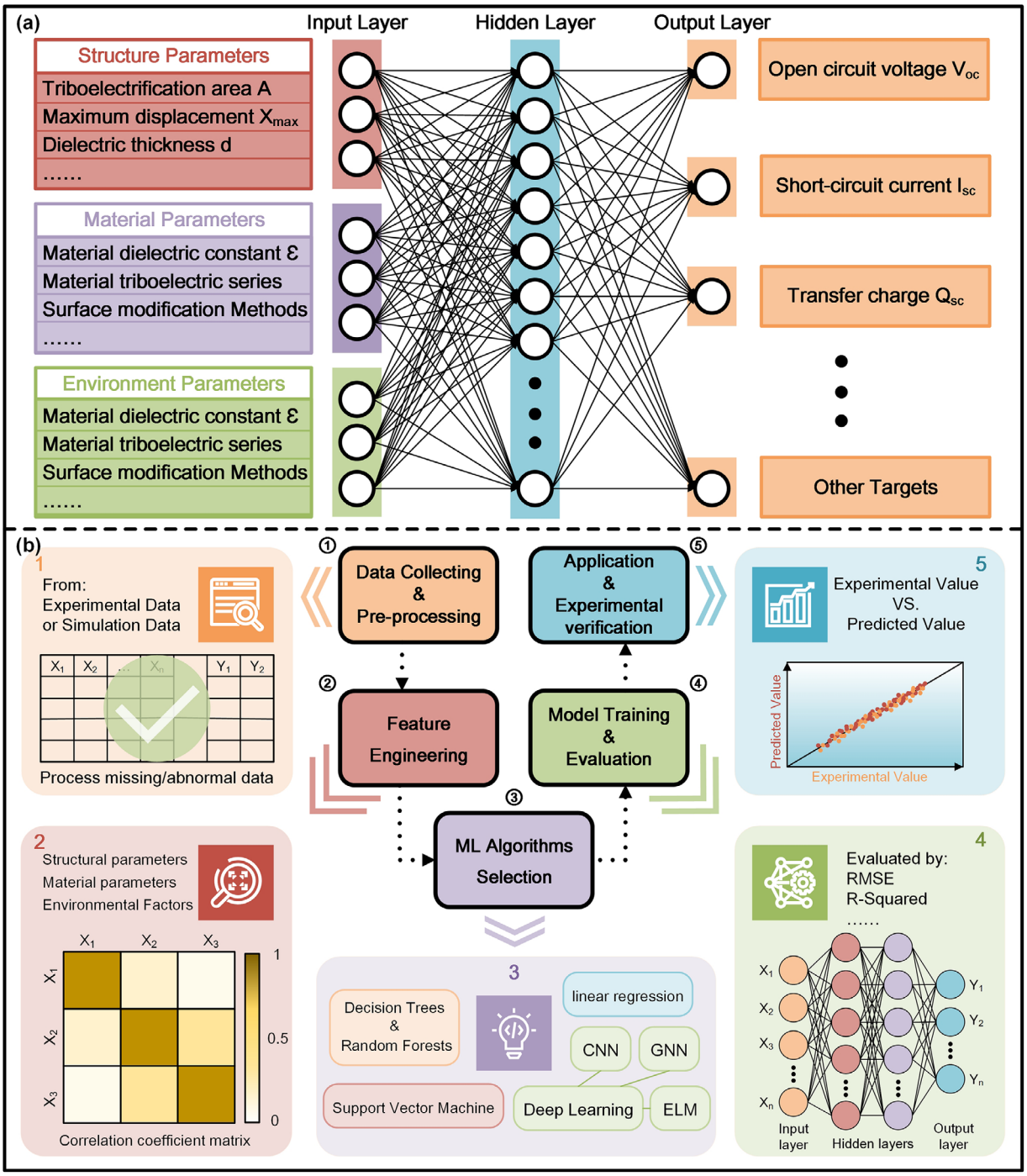

Figure 5. The general parameters and general process of TENG ML. a) A feature and target framework based on neural networks. b) The general process of ML.

4.3.2. Material Parameters

Research on the FOM_M of TENG indicates that the triboelectric charge density σ is a decisive factor.[87] Optimizing this value of σ can significantly enhance the performance of TENG, thus it is considered as a crucial material parameter. This charge density is influenced by the triboelectric properties of the friction materials. However, when quantifying the triboelectric series, the contact between solids is affected by the status of contact intimacy caused by surface roughness at the nano/micrometer level, which results in the measured surface charge density unable to reach its optimal value. To address this issue, typical liquid metals (e.g., liquid gallium, Galinstan, and mercury), can be utilized as alternative triboelectric materials to improve the contact intimacy.[87] Using

this method, Zou et al.[90] employed liquid metal mercury as a triboelectric material to establish standards for measuring the triboelectric charge density (TECD) of various materials. They subsequently measured the TECD of an array of polymers. The TECD was normalized to reflect the inherent physical properties of the material, referred to as the triboelectric series. Furthermore, Zou et al.[91] conducted measurements on the triboelectric series of over 30 inorganic non-metallic materials. The normalized value of triboelectric series serves as a crucial material parameter with significant reference implications for TENG performance. If the ML-targeted materials fall within the aforementioned triboelectric series, the quantified values can be utilized as input parameters.

The performance of TENG is significantly influenced by the surface charge density, which is affected by triboelectric charge density and the status of air/dielectric breakdown. In the parallel plate TENG model, it is critical to guarantee that the gap voltage V_{gap} under short-circuit conditions is less than the gas breakdown voltage V_b to prevent air breakdown. Research[89,92] has demonstrated that the value of V_{gap} is contingent upon the dielectric constant ε_r and the thickness d of the dielectric material. Li et al.[93] further confirmed that an optimal dielectric constant and increased thickness of dielectric materials can enhance charge density, through both theoretical derivation and empirical verification. Bulathsinghala et al.[94] conducted a comprehensive theoretical and experimental analysis on the influence of material dielectric constant on TENG performance, revealing the load-dependent nature of the TENG response to increasing dielectric constant of its layers. Under low load or short circuit conditions, a higher dielectric constant slightly improves output, while under higher loads, a lower dielectric constant notably enhances the performance. The overall maximum power output and optimal load are also higher when the dielectric constant is reduced.

Furthermore, optimization of the key materials in TENG can significantly enhance its output performance. Common strategies include surface physical modification, which increases both surface roughness and contact area.[95–98] Chemical functional group modification is another approach that enhances surface triboelectric efficiency and broadens the range of material selection.[99–103] High dielectric material doping is also employed to augment charge storage capacity,[104–106] while charge injection is utilized to increase initial surface charge density.[107–109] It is imperative to consider the critical materials with optimization strategies in feature selection to optimize ML performance.

4.3.3. Environmental Parameters

In addition to incorporating device structure and material properties into feature selection within ML, it is imperative to also consider a range of complex environmental factors. These include variables such as temperature, humidity, and atmospheric pressure.

The dielectric properties of triboelectric materials typically exhibit temperature-dependent alterations. For instance, Wen et al.[110] conducted an initial study on the performance of a TENG device within the temperature range of 77–500 K. The findings indicated that its output performance initially escalated before diminishing with rising temperature, achieving optimal performance ≈260 K. Lu et al.[111] further examined the performance fluctuations of a single-electrode TENG in the temperature range of −20 to 150 °C, revealing a consistent decrease in performance as temperature increases. The observed decline can be attributed to alterations in the dielectric properties of the material, coupled with fluctuations in effective defects under varying temperatures.

Alterations in environmental humidity can also influence the surface properties of triboelectric materials. For instance, a rise in humidity may result in an increased number of water molecules adsorbing onto the material's surface, subsequently impacting its triboelectric performance. Nguyen et al.[112] observed that as the relative humidity (RH) dropped from 90% to 10%, the charge generated by TENG (utilizing aluminum and polydimethylsiloxane as triboelectric materials) surged by over 20%. Wang et al.[113] delved into the performance of common triboelectric materials under varying RH conditions. Contrary to the conventional belief that lower RH correlates with superior triboelectric performance, their research indicated that different triboelectric materials possess distinct optimal RH values. The majority of these optimal RH values fall between 28% and 35% (with few presenting the optimal RH at 53%).

Air pressure is a critical environmental parameter due to its significant influence on the performance of TENG. Nguyen et al. have posited that as RH values approach zero, a decrease in air pressure decreases from ambient levels to 50 Torr, which will lead to a reduction in charge generation.[48] Furthermore, research indicates that the impact of air breakdown can be mitigated in high vacuum environments,[92,114] thereby significantly enhancing the performance of TENG.

4.3.4. Specific Parameters under Different Working Modes

The aforementioned general parameters for ML (encompassing structural, material, and environmental parameters) are universally applicable across all TENG operational modes. To enhance the specificity of the ML model, it is imperative to further extract the unique features of TENG across different working modes.

Given the variations in the structure and operational methods of TENG across different working modes, there is a great potential for selecting input parameters during the ML process. For instance, TENG in contact-separation and lateral sliding modes, the effective dielectric thickness d_0 emerges as a crucial parameter, as defined by the formula:[115,116]

$$d_0 = \frac{d_1}{\varepsilon_1} + \frac{d_2}{\varepsilon_2} \tag{2}$$

In this context, d_1 and d_2 represent the thicknesses of the two dielectric materials, while ε_1 and ε_2 denote their respective dielectric constants.

In the context of freestanding TENG, two critical parameters, the freestanding height h and the electrode gap g, exhibit a significant coupling effect on its output performance.[117] These parameters can be regarded as pivotal features in ML. Similarly, for single-electrode TENG, a robust correlation on TENG output exists depending on the distance g from the single electrode to the reference electrode.[118] Furthermore, the properties of the reference electrode, inclusive of structural parameters such as its

Table 2. ML parameters of TENG optimization for reference.

Parameter types	Parameters	Applicable TENG	Refs.
Structure	Maximum displacement distance	All	[87,120]
	Contact area of device		
	Thickness of the dielectric layer		[89]
	Load resistance		[120]
	Electrode gap distance	SE, FT	[117,118]
	Properties of reference electrodes	SE	[119]
	Hight of free layer	FT	[117]
Material	Material dielectric constant	All	[93]
	Triboelectric sequence		[90,91]
	Surface treatment		[95–109]
	Effective thickness of dielectric layers	CS, LS	[115,116]
	Ambient temperature	All	[110,111]
Environment	Ambient humidity		[112]
	Ambient pressure		
Other factors	Average velocity of contact-separation	CS	[115]
	Period of Motion	CS, LS	[116,120]
	Sliding acceleration	LS	[116,121]
	Sliding velocity		[122]
	Dynamic friction coefficient		
	Apply force		

position, area, thickness, and shape, significantly influence the overall performance of the equipment.[119]

In addition to material parameters, structural parameters, and environmental factors, the operating conditions under various working modes can significantly influence the output of TENG. The velocity,[115,122] acceleration,[116,121] and period of motion[117,120] during TENG's operation can also be considered as input parameters. A comprehensive list of different types of ML parameters for TENG is provided in **Table 2** for reference.

4.4. The General Process of ML

As illustrated in Figure 5b, the overarching process of ML technology can be delineated into five distinct steps: 1) The collection and preprocessing of data. 2) The execution of feature engineering to discern significant input parameters. 3) The selection of an appropriate ML algorithm. 4) The training and evaluation of the ML model. 5) The application of the optimally trained model to prediction, followed by experimental verification.

4.4.1. Data Collecting and Pre-Processing

Dataset quality determines ML outcomes due to its direct impact on prediction accuracy. Typically, ML data in the domain of energy harvesting and storage devices primarily originates from published experimental records or computational simulations. For material property analysis, established authoritative databases like the materials project,[123] industrial crystal structure database,[124] and crystal open database[125] provide validated references. When experimental datasets with sufficient quality and statistical representativeness exist in the target domain, their direct utilization offers cost-efficiency advantages. Conversely, under scenarios involving scarce experimental data, prohibitive costs, or extreme operational conditions, simulation-based approaches emerge as viable alternatives. TENG data acquisition strategies are determined by both the requirements of research objectives and the quality/quantity of available data in relevant literatures. If a substantial volume of published data exists pertaining to the research objective type, or if the experimental conditions are readily attainable, data can be produced from the actual experimentation. Since TENG performance exhibits sensitivity to minor parameter fluctuations, it is imperative to ensure the reproducibility of these experimental data. When existing data is insufficient and experimental data collection is challenging, mathematical models and simulation tools (e.g., COMSOL Multiphysics) can be utilized to generate simulated datasets.

ML applied to TENG performance prediction requires systematic integration of multi-domain parameters. The characteristic parameters include structural parameters such as maximum displacement area, device area, dielectric layer thickness, and load resistance; material parameters like triboelectric series, dielectric constant, and the optimization of the material; environmental parameters encompassing temperature, humidity, and air pressure; output performance metrics include V_{OC}, I_{SC}, Q_{SC}, and output power.

Upon completion of data collection, it is essential to perform data preprocessing. If the data originates from published literature, discrepancies in the types of contained data may lead to missing values in the resulting dataset. Depending on the types of parameter types, there are relevant strategies for dealing with the missing data. For numerical TENG parameters (e.g., dielectric thickness), statistical imputation (e.g., mean or median

substitution) proves effective. When the missing data exceeds a certain threshold (such as 30%), this data set should be deleted. Non-numerical discrete features may also be encountered, which require transformation through encoding schemes prior to model ingestion. An example could be the optimization methods for triboelectric materials in TENG, which encompass surface physical modification, surface chemical modification, and high-κ material doping. Prior to incorporating these parameters into ML algorithms, it is imperative to convert these features into numerical formats comprehensible to the model. Common techniques for this conversion include label encoding or one-hot encoding. Notably, one-hot encoding proves more apt for classifying different material optimization methods, given their lack of mutual relationships.

Feature scaling (including normalization/standardization) is a crucial aspect of data preprocessing, as it markedly enhances the performance of ML algorithms and expedites the training process. This is particularly true for gradient descent-based algorithms, such as LR and ANN, as well as distance-based algorithms like K-nearest neighbors and K-means. Feature scaling is essential in these scenarios to ensure that data points are on comparable scales. This approach mitigates issues arising from scale discrepancies, thereby facilitating a more robust and efficient learning of feature relationships.

4.4.2. Feature Engineering

In ML, features generally refer to the various attributes or variables used to describe samples in data, also known as fingerprints or descriptors in literature.[126] Features are also the basis for ML models to learn patterns and make predictions from data. They contain useful information related with samples, which can be in the form of numerical values, categories, text, images, etc. The objective of feature engineering is to extract optimal features from raw data that enhance target analysis, while reducing dimensionality without sacrificing model performance. In the context of high-dimensional data, dimensionality reduction methods are typically employed to mitigate redundant information and enhance the model's generalization. Commonly used dimensionality reduction techniques include principal component analysis[127] and t-distribution neighborhood embedding.[128] For TENG-optimized models, the number of features is relatively small, allowing for the adoption of feature selection methods to optimize the feature set. The prevalent method of feature selection involves the analysis of data correlation, which is bifurcated into two categories: the correlation between features and the correlation between features and targets. An ideal feature set exhibits low inter-feature correlation (minimizing multicollinearity risks that compromise model stability and interpretability) and high feature-target correlation (maximizing predictive accuracy). Excessive feature redundancy also increases computational costs.

4.4.3. ML Algorithms Selection

The second section of this paper introduces several prevalent ML algorithms utilized for material screening and device optimization. There is no specific algorithm that is superior to all other algorithms in solving different problems,[129] so it is necessary to choose the appropriate algorithm based on the specific target. The choice of ML algorithms depends on data characteristics (scale, dimensionality, noise, etc.), task objectives (classification, regression, clustering, etc.), structural complexity (nonlinearity, sparsity, etc.), and deployment constraints (interpretability, computational resources, etc.). For predicting the performance of TENG devices, data is typically structured in tabular format with numerical features. Given that the relationship between features is often non-linear, linear regression models, which are relatively simplistic, are unsuited for such predictions. In most instances, tree-based ML models (DT and RF) prove more effective for predicting TENG performance under identical working modes due to their suitability for tasks with low feature dimensions and relatively small datasets. However, when dealing with complex feature relationships and large datasets, deep learning emerges as a viable option. Despite the lack of interpretability compared to DT and RF, deep learning boasts superior adaptability to complex patterns and generalization to unseen data. Given the diverse parameter configurations and experimental conditions associated with different problems, the most effective strategy for determining the optimal ML algorithm for a given problem involves experimenting with multiple algorithms and conducting a comprehensive evaluation.

4.4.4. Model Training and Evaluation

Model training is a process designed to enable the ML algorithm to fully comprehend the patterns within the data, and subsequently adjust the model's parameters (such as weights and biases) through repeated iterative training. The ultimate objective of this process is to minimize the loss function by adjusting parameters (e.g., weights and biases), thereby enabling the model to generalize well to unseen data. To achieve this goal, systematic tuning is required. Hyperparameters, which include both training settings (e.g., learning rate, number of epochs) and architectural choices (e.g., hidden layer size, activation functions), play a critical role.[130] Properly tuning these values controls model complexity. For instance, higher learning rates accelerate convergence but risk instability, while deeper networks improve fitting capacity at the cost of overfitting. Since datasets vary in characteristics and distributions, properly tuned hyperparameters enable the model to adapt to these variations, balancing between underfitting and overfitting. In traditional ANN training, the SGD method[131] is commonly employed to optimize the training model. However, adaptive algorithms like root mean square propagation and adaptive moment estimation are now widely adopted. These methods adjust learning rates per parameter, enabling faster convergence and robustness to hyperparameter choices. Beyond gradient-based methods, evolutionary algorithms (e.g., GA, PSO, GWO) offer a global search strategy to optimize both hyperparameters and network architectures (e.g., depth, width), albeit at higher computational costs.

During the training phase of the optimal model, evaluation metrics provide quantitative feedback during hyperparameter tuning, guiding the selection of configurations that maximize model performance. For regression models forecasting TENG performance, prevalent evaluation metrics encompass

mean square error, root mean square error (RMSE), MAE, R^2. Complementing these metrics, techniques such as K-fold cross-validation and diagnostic visualizations are applied to holistically evaluate model performance. K-fold cross-validation mitigates overfitting by evaluating hyperparameters across diverse data splits, ensuring their robustness to data variability. Visualizations like scatter plots (actual versus predicted values) reveal systematic biases, while residual plots highlight regions where the model underperforms.

4.4.5. Application and Experimental Verification

The final phase entails experimental validation of the model's predictive capability under diverse combinations of material, structure, and environmental parameters. Once the performance of the model has been validated, it can be utilized to predict TENG performance for new datasets. It is crucial to underscore that the efficacy of TENG is significantly influenced by certain environmental conditions, including temperature and humidity. Consequently, it is imperative to maintain consistency between the parameters in the experimental design and those in the model's input.

5. ML for SC Performance Optimization

In SCPS, the performance of energy-storage devices can also be optimized through ML. There have been many studies exploring how to improve the performance of batteries and SCs assisted with ML. This section will take SC as the typical energy-storage device and give a comprehensive investigation, from the basic working principle to the progress of carbon-based SC design based on ML technology and computer-aided solution to self-discharge problem.

5.1. Supercapacitors

Compared with large-scale power grid energy-storage systems, portable and wearable electronic devices rely even more on the support of SCPS. The potential applications of SCPS in the future will be vast, for which the effective enhancement of their performance will be a critical issue.[9,132–135] In the previous sections, we have systematically explored and anticipated strategies to improve the performance of TENG through a ML approach. Beyond enhancing the energy-harvesting properties, it is essential to augment the storage capacity of SCs at the energy-storage side. Concurrently, addressing the inevitable self-discharge phenomenon inherent in SCs is crucial for achieving cost-effectiveness.[136–141]

SCs are devices designed to address the escalating energy demand. They have gained great attention from researchers due to their high power density and safe operation.[142–144] The longevity of SCs is a crucial parameter for a SCPS, which aims to provide sustainable energy. The energy storage mechanism of the SC is illustrated in **Figure 6a**. During the charge-discharge process of the electrical double layer (EDL) SC, the electrolyte ions move in opposing directions without any chemical reaction. This allows the EDL SC to maintain excellent electrochemical performance over tens of thousands of cycles. However, an energy storage process relying solely on a physical energy-storage mechanism results in a low specific capacitance value for the EDL SC. As illustrated in Figure 6b, a pseudocapacitor undergoes a Faradaic redox reactions between the electrode material and the electrolyte ions during charge-discharge processes. This unique energy storage mechanism allows the pseudocapacitor to deliver a higher specific capacitance. The process is characterized by a swift, reversible redox reaction at or near the active material's surface. This mechanism is related to a shift in the electrode material's valence state due to electron transfer. However, the sluggish rate of the Faradaic reaction compared to the charge electrostatic adsorption and detachment rate results in a low power density for the pseudocapacitor and poor cycling performance. Currently, the electrode material is the primary factor influencing the performance of SCs.

The self-discharge phenomenon of SCs results in a swift voltage drop and energy loss within the energy-storage device. Therefore, comprehending the mechanism of self-discharge is vital to mitigate the adverse effects induced by this behavior.[145–148] To date, three commonly accepted mechanisms for self-discharge have been widely accepted: leakage current, Faradaic reaction (Figure 6c), and charge redistribution (Figure 6d). The leakage current primarily arises from redox reactions near the electrode-electrolyte interface and internal short-circuiting of the device during the assembly process. Conversely, the Faradaic reaction predominantly occurs due to the redox reaction between the functional groups of the carbon-based material and the electrolyte, leading to a voltage drop in the SC. Charge redistribution, in contrast, is attributed to the charge concentration in the pores when the SC is in its filled state, which then migrates toward the depth of these pores due to concentration differences. This migration is hindered by strong resistance, resulting in more obstruction to ion movement within the pores than that within the electrolyte. This is the reason why spontaneous voltage drop occurs. These three reasons to the self-discharge behavior in SCs are closely tied to electrode materials. Carbon-based electrode materials have thus far been extensively utilized in SCs, underscoring the significance of suppressing their self-discharge. Consequently, it is imperative to minimize and prevent self-discharge generated by these carbon-based materials.

5.2. ML for Carbon-Based SCs

Liu et al.[149] have leveraged ML techniques, utilizing hundreds of experimental data points from the literature, to propose a novel approach for designing high-efficiency carbon materials for SCs. The primary focus is to investigate the correlation between pore structure and SC capacitance (**Figure 7a**). The predicted capacitance of these carbon-based materials is achieved through six ML models: extreme gradient boosting (XGBoost), gradient boosting machine, RF, multiple linear regression, SVM and ANN. Notably, XGBoost model demonstrates superior predictive performance with an accuracy of 0.892, surpassing the other models. Among various parameters influencing porous features, specific surface area (SSA), pore size (PS), and micropore surface area percentage are found to have the most significant impact on capacitance performance. This methodology significantly

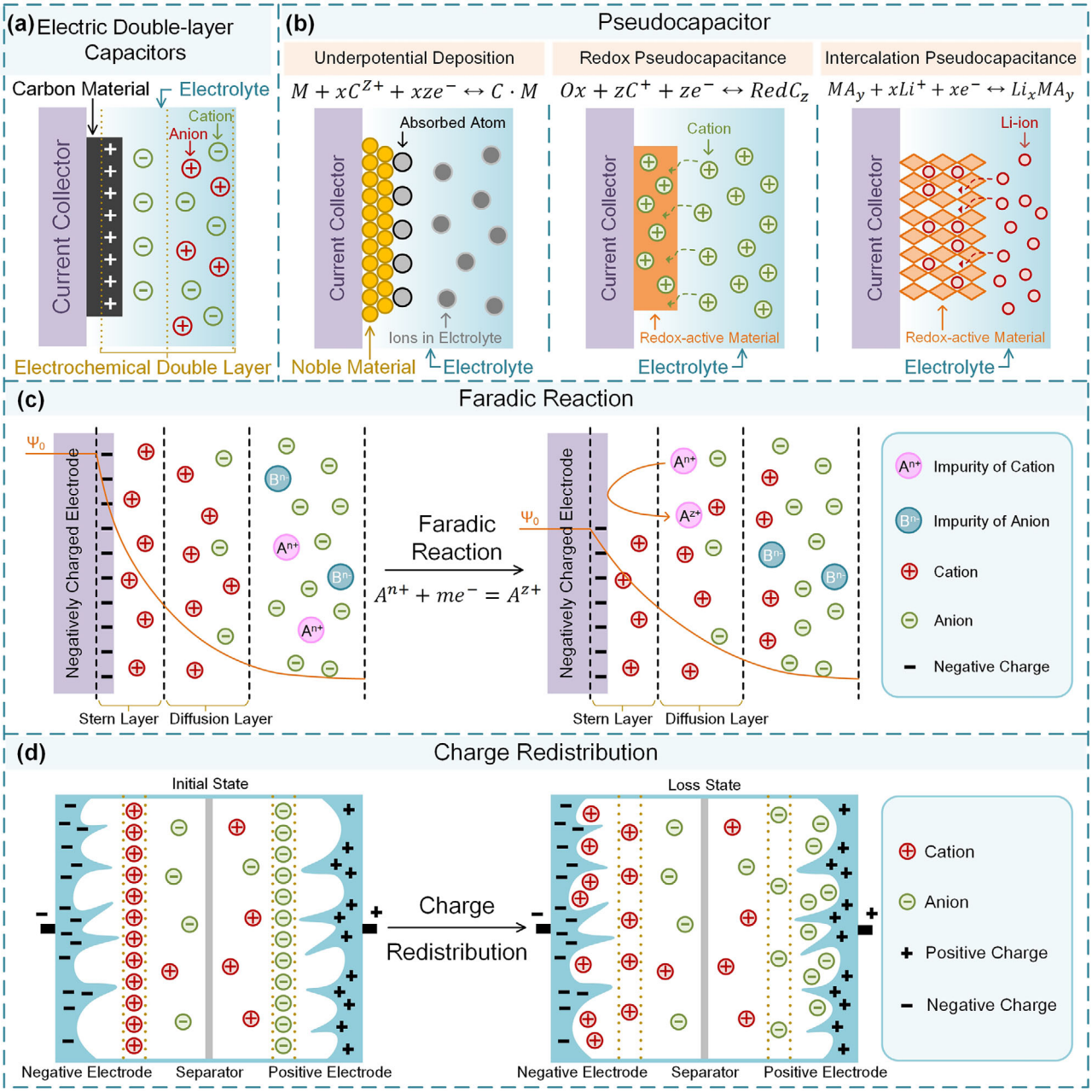

Figure 6. Energy storage and self-discharge mechanisms of supercapacitors. a) Bilayer b) underpotential deposition, redox, and ionic embedding. c) Faradaic reaction d) Charge redistribution.

reduces both the cost and time associated with experimental procedures, delivering a promising direction for future research on how to design high-performance carbon-based electrode materials. Kushwaha et al.[150] reported on the prediction of the capacitance performance for carbon-based SCs using five ML models. Several parameters, including voltage window, specific surface area (m^2 g^{-1}), and the pore size (nm), are selected to evaluate their contributions and effects on capacitance. The results indicate that the ANN model provides the most accurate predictions, exhibiting the least RMSE and MAE, as along with the highest R^2-score values. The performance of the XGBoost and RF regressor models closely matches that of the ANN model. Wang et al.[151] introduced a ML-guided activation strategy for carbon materials. The capacitance performance of SC was optimized by adjusting the pore size structure and oxygen content within the carbon material. This approach closely aligns with the specific capacitance of porous carbon electrodes, as predicted by ML methods.

In addition to the pore size/structure of the carbon-based materials, heteroatom-containing functional groups significantly influence the capacitive performance of SCs. This can typically be modified by doping with heteroatoms such as nitrogen, oxygen, and sulfur into carbon electrodes. Furthermore, doping nitrogen

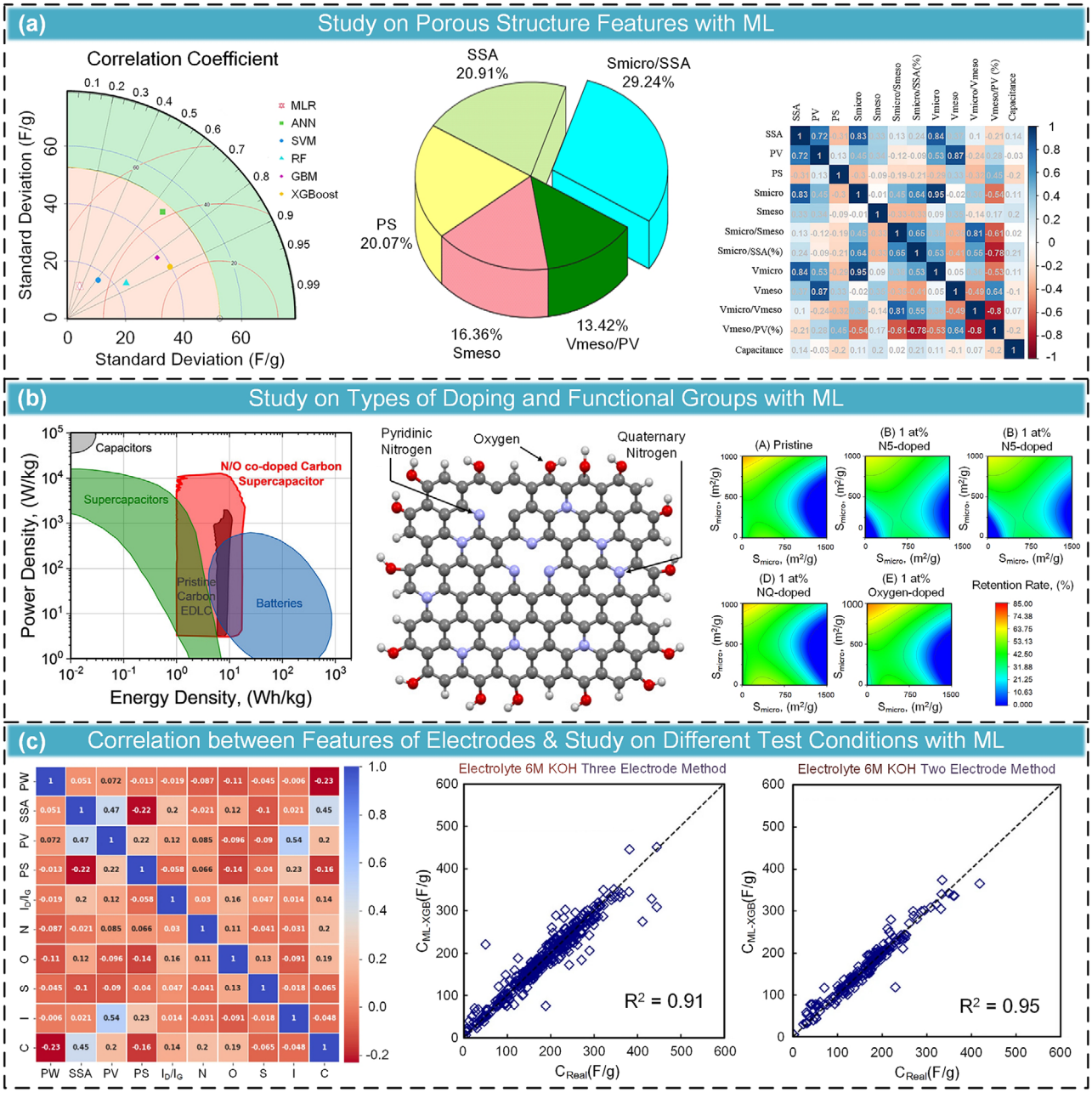

Figure 7. ML guided SC carbon material design. a) Statistical comparison of six model estimates of Taylor diagrams, the share of porous structure features on the specific capacitance predicted by the XGBoost model, and the Pearson's correlation coefficient between the porous structure features and the specific capacitance. Reproduced with permission.[149] Copyright 2021, Elsevier. b) Heteroatom doping types, and the effect of different types of functional groups on the capacitance predicted by the ANN. Reproduced with permission.[152] Copyright 2020, American Chemical Society. c) Correlation between physicochemical properties of the carbon electrodes of supercapacitors. Comparison between predicted and actual specific capacitance under different test conditions. Reproduced with permission.[155] Copyright 2023, The Authors.

on the carbon material acts as an electron donor, thereby enhancing specific capacitance and improving the wettability of the material via the Faradaic reaction. Zhou et al.[152] have elucidated how the surface functional groups on carbon materials impact the performances of SCs. The ML model offers a comprehensive guide for designing and developing heteroatomic carbon materials, potentially leading to a substantial increase in the energy storage capacity of carbon-based materials (Figure 7b). Zhu et al.[153] have assembled a dataset from over 300 literature sources on carbon-based SCs, extracting more than 680 valid points. They have selected five key features to analyze and assess their impact on capacitance, including the specific surface area, evaluated pore size, N doping level, voltage window, and I_D/I_G ratio (the intensity ratio of the D-band to the G-band in Raman spectroscopy). The findings indicate that the predictions made by ANN outperform those of linear regression and LASSO regression. This

research underscores the significant potential of ANN in materials science and application design. Su et al.[154] have employed ML techniques to predict the capacitance of carbon-based SCs. The gathered 121 sets of data are collected to incorporate with seven variables: pore volume, pore size, specific surface area, N and O doping percentage, potential window, and I_D/I_G ratio. The influence of these variable parameters on the bilayer's capacitance was examined using four typical ML models. The performance ranking of these models is as follows: RT > multilayer perceptron > SVR > LR.

The final capacitance performance is also influenced by various test conditions and electrolyte types. Mishra et al.[155] have examined the impact of electrode material characteristics on the capacitance by analyzing the experimental data from 147 literature sources (comprising 4899 feature data) and establishing a database for training and evaluating their ML model. This analysis incorporated previously documented features, including pore volume, pore size, defect presence, specific surface area, O and N content, current density, and potential window. Furthermore, they considered categorical variables like testing method, electrolyte type, and electrode carbon structure. The XGBoost model was employed to predict the influence of two-electrode and three-electrode characterizing strategies on the specific capacitance of SCs. The findings demonstrated satisfactory performance parameters for both testing methodologies. To elucidate the relationship between electrolyte and specific capacitance, datasets were extracted from both the characterizing methods using an electrolyte of 6 M KOH. Performance parameters derived from the XGBoost method revealed that pore volume, SSA, and N% significantly influenced the three-electrode testing method, whereas SSA, PS, and potential window were identified as significant contributors to the two-electrode method. This research provides a foundation for future analysis and optimization of carbon-based SCs' specific capacitance. It also offers insights into the chemical characterization and structure of carbon-based materials, as well as the impact of testing methods and electrolyte on the capacitance (Figure 7c). Saad et al.[156] conducted an extensive study of over 200 articles on carbon-based SCs, culminating in the creation of a corresponding database. Concurrently, they gathered 15 distinct parameters with the objective of developing a predictive model that could account for all conditional inputs. The specific capacitance is influenced by several physicochemical properties of the electrode material, including electrode configuration, SSA, pore size/volume, the percentage of C, N, and O atoms, and the ratio of I_D/I_G. Furthermore, the specific capacitance is also affected by the electrochemical characteristics derived from GCD tests and EIS analyses. These include cell configuration, electrolyte concentration, electrolyte ionic conductivity, applied potential window, current density, charge-transfer resistance, and equivalent series resistance. The ANN model demonstrates a robust capability to generate high predictive accuracy values of 60.42 and 0.88 for the lowest RMSE and the largest R^2, respectively.

5.3. The Self-Discharge of SCs

To date, the literature reports on the enhancement of carbon-based SCs have seen a consistent annual increase, with SCs gaining significant traction in the realm of energy storage. Nevertheless, it is imperative to acknowledge that pronounced self-discharge remains a pivotal challenge in SC applications.[157]

Despite the paucity of information on how ML guides the material design and predicts self-discharge properties in SCs, a significant volume of literature on SC modeling has been published in recent years.[135,158,159] A primary impetus for this surge in modeling research is that precise models facilitate an understanding of the self-discharge behavior of SCs under diverse scenarios, obviating the need for physical experiments. This could significantly reduce the time and cost for relevant research. This section primarily concentrates on the development of various self-discharge models for SCs, as well as the strategies reported to alleviate the self-discharge phenomenon in carbon-based SCs.

Pourkheirollah et al.[160] introduced a straightforward numerical index-based means to simulate SCs' self-discharge behavior (**Figure 8a**). By employing experimental data from SCs to model this self-discharge process, they were able to accurately replicate the fixed curves of both self-discharge and leakage, thereby predicting the long-term self-discharge behavior of SCs with high precision. This methodology is not only efficient but also universally applicable to carbon-based SCs. Kunwar et al.[161] further elucidated the energy-storage mechanism of SCs through a simplistic self-discharge curve (Figure 8b). These self-discharge curves were plotted assisted with the MATLAB/Simulink platform, with experiments conducted to record the self-discharge curves of various electrode materials and different types of electrolytes. The experimental data align well with the simulation data. This model employs a straightforward data extraction algorithm, comprised of three distinct models: rapid branching for short-term behavior, slow branching, and long-term behavior simulation with leakage resistance. The efficacy of the model was ascertained by simulating its charge/discharge behavior and implementing a comparison with experiment data. The proposed model is particularly well-suited for understanding the self-discharge behavior simulations. Kaus et al.[162] introduced a complex electrical model to address the charge redistribution mechanism of SC self-discharge. The model they developed effectively predicted the impact of initial voltage, charge duration, and temperature on open circuit voltage decay. The predictions align closely with experimental results. Ghanbari et al.[163] presented a dynamic simulation on the equivalent circuit of SC by utilizing the experimental data extracted from self-discharge behavior. The optimal exponential function was determined through the weighted least squares method and fitted to this data. This model provides an effective balance between accuracy and simplicity. Tevi et al.[146] constructed a mathematical model to simulate and demonstrate the impact of blocking on the self-discharge performance of SCs. Kowal et al.[164] elucidated the self-discharge mechanism of SCs using a straightforward equivalent circuit model (**Figure 9**).

Self-discharge significantly impedes the practical application of SCs. To address this issue, a range of innovative and viable strategies have been proposed to mitigate self-discharge based on the underlying mechanism. Li et al.[165] developed activated carbon electrodes with varying mass loadings and examined the impact of different loadings on the self-discharge behavior of SCs. The experimental findings indicate that as the mass loading increases, the attenuation of the open-circuit voltage decreases.

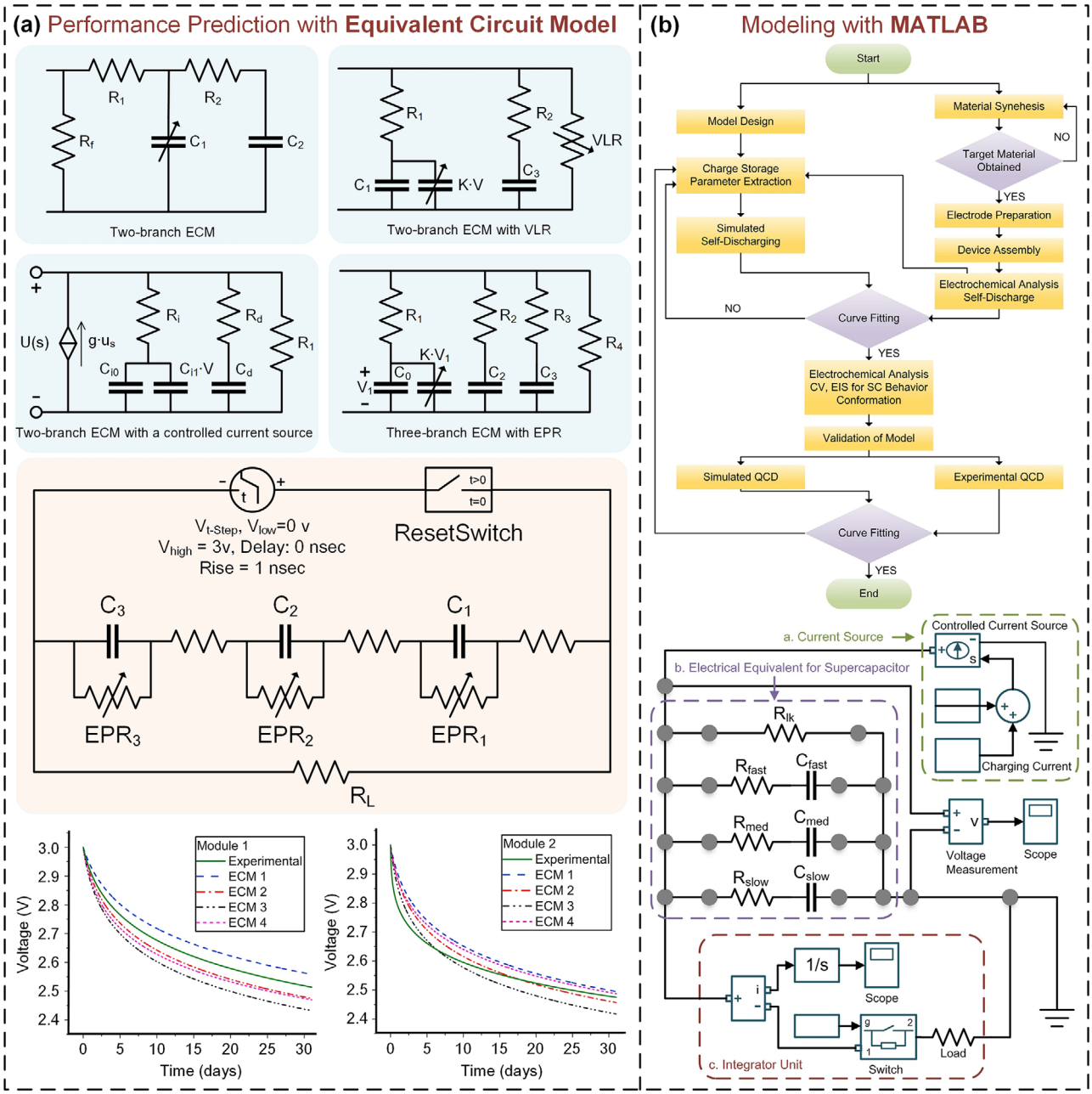

Figure 8. Self-discharge phenomenon and computer modeling of supercapacitors. a) Experimental and simulation results of ECM, self-discharge behavior of SC. Reproduced with permission.[160] Copyright 2023, The Authors. b) Overall approach to develop supercapacitor test system based on self-discharge data, MATLAB unit supercapacitor models. Reproduced with permission.[161] Copyright 2023, Elsevier.

Specially, when the activated carbon loading escalates from 0.6 to 10.6 mg cm^{-2}, the voltage attenuation diminishes from 1.07 mV to 0.05 mV mF^{-1} h^{-1}. Nitrogen-rich groups appear to be more effective in inhibiting self-discharge compared to oxygen-rich ones. This is particularly true for reduced graphene oxide material, which possesses both porous and high nitrogen content and exhibits a low self-discharge rate. This phenomenon can be explained by the interaction between the electrolyte ions and the nitrogen-containing functional groups. This binding force impedes the redistribution of ions, thereby reducing the self-discharge process. Despite recent advancements in mitigating the self-discharge of SCs, there remains a need for more straightforward and efficient strategies to further diminish this phenomenon. Xia et al.[145] proposed a method to reduce SCs' self-discharge, leveraging the electrorheological (ER) effect. This approach involves incorporating ER molecules into the electrolyte, such as 4-n-pentyl-4′-cyanobiphenyl (5CB, a nematic liquid crystal characterized by high dielectric anisotropy and chemical stability). Upon application of an electric field, the 5CB molecules align in a specific direction of approximately parallel long axes.

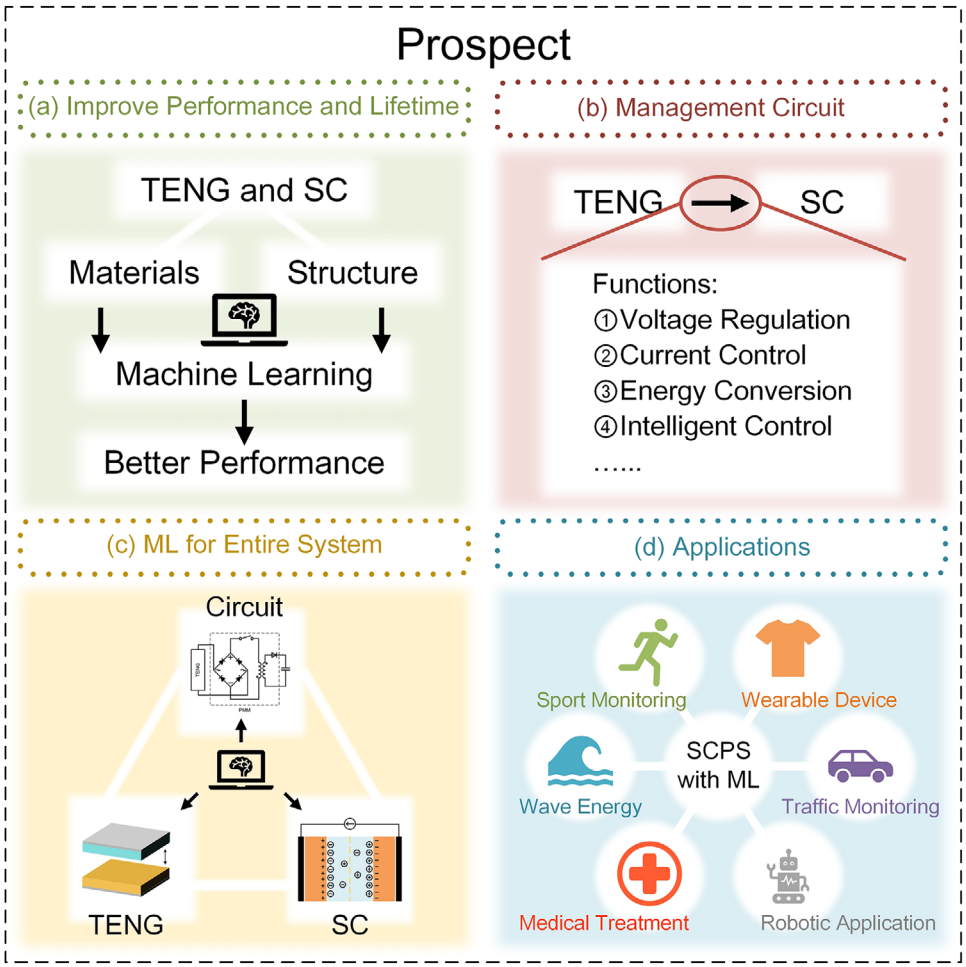

Figure 9. Prospects of SCPS based on TENG and SC. a) ML-assisted device performance optimization. b) Management circuit design with ML. c) ML integration for the entire system. d) ML-enabled SCPS for diverse applications.

This alteration in molecular alignment results in a swiftly increased fluid viscosity, which can be controlled by applied external electric field. This mechanism effectively mitigates the self-discharge effect of SCs. Consequently, this low leakage current SC can be synergistically integrated with TENG to enhance the charging efficiency of SC. The separator constitutes a crucial component of SCs, serving a pivotal role in preventing internal short circuits and facilitating the development of safe and high-performance SCs. Wang et al.[166] introduced an innovative modification to the separator by incorporating sulfonate ion exchange resin. This modified configuration enables the effective capture of impurities (specifically transition metal ions) in the electrolyte. Consequently, this minimizes self-discharge, thereby improving the overall performance and reliability of the SCs.

SCs experience spontaneous charge loss and voltage drop, resulting in a prevalent self-discharge. This process significantly hinders the practical application of SCs, although it is not entirely feasible to eliminate it. The most effective approach is to minimize the rate of self-discharge as much as possible. Current strategies for suppressing self-discharge primarily involve modifying electrode materials, adjusting electrolyte, and regulating the separator. As research into the phenomenon and theory of SC self-discharge continues to expand, ML will undoubtedly play a pivotal role in this field. As a critical factor influencing the performance of SCs, self-discharge mechanism necessitates in-depth analysis and understanding assisted with ML technology. The robust data processing and pattern recognition capabilities of ML offer effective means to elucidate the complex mechanisms underlying self-discharge phenomena and guide the optimal design of SCs.

6. Summary and Prospective

In this review, we have presented a comprehensive review on recent advancements in integrated energy harvesting/storage systems, with particular emphasis on the progress made in SCPS based on TENG and SC. As a pivotal branch of AI technology, ML has proven its utility not only in predicting device performance but also in guiding material design through data analysis. We have collected key parameters associated with TENG performance from theoretical literatures and proposed a scheme for predicting and guiding TENG design using ML. It is anticipated that in the foreseeable future, ML will be instrumental in guiding the development of TENG. In relation to SC, our focus lies

in designing the most common and economic carbon materials using ML. This involves incorporating parameters such as pore size, functional groups, and test conditions into a learning model to predict the lifespan of SC. This approach holds significant potential for enhancing the energy storage capacity of SC. As the self-discharge phenomenon frequently observed in SC devices cannot be entirely eradicated, its impact is highly encouraged to be mitigated. This paper also discusses the mechanism and process of self-discharge based on equivalent circuit simulation. Assisted with ML analysis, the rate of self-discharge can be reduced effectively by optimizing the design of electrode materials, as well as by regulating the electrolyte and separator. We anticipate that with an increase in the amount of self-discharge research, there will be more effective data to construct a complete synergistic database for pursuing ML-enhanced SCPSs.

Despite the notable advancements in SCPS, we believe that the swift progression of artificial intelligence will not only continue to facilitate the development of the self-powered devices/systems but also guide the ML-assisted design and optimization of materials and device structures. Until now, there are still some critical concerns remaining to be explored within this domain.

6.1. Device Performance and Lifetime

The primary concern in the realm of energy-harvesting components is their efficiency. The performance of TENG is heavily reliant on the surface charge density. Further research should focus on enhancing this surface charge density, addressing issues related to air and dielectric breakdown, and optimizing dielectric materials. Additionally, for energy storage devices, it is crucial to further mitigate the self-discharge behavior of SC.

In contemporary practical applications, the longevity of SCPSs' components, especially TENG, has been a significant challenge due to material degradation. Nevertheless, these self-sustainable systems hold immense potential for future advancements. Future research is imperative to enhance the performance of each integrated unit, encompassing output power, capacitance, cycling stability, and device lifespan. ML emerges as a promising approach in optimizing structural design and material selection in enhancing SCPS performance. The use of ML technology can accelerate material screening and explore materials with higher dielectric constants and higher surface charge densities. In the future, ML can also be applied to reverse design of materials, accelerating the development of new materials. In addition, ML can be used to predict the long-term performance of materials and identify the performance degradation path of materials in advance. The current limited research on ML still focuses on optimizing the parameters of TENG structures. Moving forward, there is an urgent need to delve deeper into research and develop innovative materials and structures to bolster the performance and sustainability of SCPSs.

6.2. Management Circuit

Currently, the impedance mismatch between TENG and energy-storage devices results in suboptimal energy transfer efficiency. Consequently, there is a pressing need to enhance conversion efficiency. Charge pumps and buck converters have demonstrated high efficiency and versatility across various modes, marking significant advancements in recent years. However, the energy conversion efficiency of SCPSs remains low, necessitating further investigation. To address this challenge, it is imperative to develop and design more efficient power management circuits for TENGs. By collecting data and leveraging ML techniques, researchers can design more efficient energy management circuits. Considering the large amount of data to be collected and the complexity of experiments, ML can be combined with circuit simulation models to optimize the management circuits. By using circuit simulation software, such as LTspice, TENG can be modeled as an equivalent circuit, typically represented by a series connection of a voltage source and a capacitor. The parameters of electronic components in the circuit, such as capacitance, inductance, resistance, and diode characteristics, can be adjusted within simulation software. The software then calculates key performance indicators of the management circuit, such as energy storage efficiency, based on these adjustable parameters. By varying the combinations of these parameters, large datasets can be generated for ML analysis. The resulting ML model can then predict and analyze the performance of management circuits with different parameter combinations.

6.3. ML for the Entire System

While ML has been extensively researched and implemented across various components of SCPS, it is plausible to predict that its application will expand further in the future, particularly in the design and management of the entire self-charging or self-powered system. It is necessary to build a more intelligent SCPS system. The integration of ML into these systems should facilitate adaptive capabilities for their components, such as the ability to modify TENG's operational mode based on environmental fluctuations and real-time data. This comprehensive approach to ML will enhance the intelligence and adaptability of SCPS, thereby optimizing the performance, responsiveness, and sustainability of the entire system. In addition, future intelligent SCPS systems may involve not only power management for a single device, but also collaborative work among multiple systems. The distributed SCPS network allows multiple self-charging systems to share data and resources, optimizing overall efficiency through cross-system collaboration. Applying ML to the overall system can enable nodes to share data, and the application of multi-objective optimization algorithms can also achieve balance between multiple requirements and meet diverse application scenarios.

6.4. Application Scenarios

Utilizing ML, the application scope of SCPS can be significantly expanded, encompassing intricate functions such as image recognition and password unlocking. Furthermore, SCPS can find utility in domains like smart homes, IoT, and wearable devices, offering a sustainable power source for these technologically advanced systems. When SCPS is applied on the IoT, multiple functional devices may be included in the system. The energy collected by TENG may not be able to meet the long-term continuous power supply requirements of the entire system. ML

can be applied to analyze historical data of various load devices and predict future electricity demand, achieving intelligent energy scheduling. Future research should aim to explore and develop novel application scenarios, fully integrating ML technology with SCPSs, thereby further broadening the potential applications of SCPSs.

Acknowledgements

This work is supported by the National Natural Science Foundation of China (52073031), the National Key Research and Development Program of China (2023YFB3208102), and the "Hundred Talents Program" of the Chinese Academy of Sciences.

Conflict of Interest

The authors declare no conflict of interest.

Keywords

machine learning, parameter optimization, self-charging power source, supercapacitors, TENGs

Received: March 4, 2025
Published online:

[1] L. Atzori, A. Iera, G. Morabito, *Comput. Netw.* **2010**, *54*, 2787.
[2] S. Seneviratne, Y. Hu, T. Nguyen, G. Lan, S. Khalifa, K. Thilakarathna, M. Hassan, A. Seneviratne, *IEEE Commun. Surv. Tutorials* **2017**, *19*, 2573.
[3] Z. Wang, *Sci. Am.* **2008**, *298*, 82.
[4] G. Zhu, R. Yang, S. Wang, Z. L. Wang, *Nano Lett.* **2010**, *10*, 3151.
[5] J. Bae, Y. J. Park, M. Lee, S. N. Cha, Y. J. Choi, C. S. Lee, J. M. Kim, Z. L. Wang, *Adv. Mater.* **2011**, *23*, 3446.
[6] F.-R. Fan, Z.-Q. Tian, Z. L Wang, *Nano Energy* **2012**, *1*, 328.
[7] X. Xiao, T. Li, P. Yang, Y. Gao, H. Jin, W. Ni, W. Zhan, X. Zhang, Y. Cao, J. Zhong, L. Gong, W.-C. Yen, W. Mai, J. Chen, K. Huo, Y.-L. Chueh, Z. L. Wang, J. Zhou, *ACS Nano* **2012**, *6*, 9200.
[8] X. Pu, Z. L. Wang, *Chem. Sci.* **2021**, *12*, 34.
[9] J. Luo, Z. L. Wang, *Energy Storage Mater.* **2019**, *23*, 617.
[10] S. Li, Z. Li, X. Wan, Y. Chen, *eScience* **2023**, *3*, 100085.
[11] T. Cheng, J. Shao, Z. L. Wang, *Nat. Rev. Methods Primers* **2023**, *3*, 39.
[12] T. Cao, X.-L. Shi, M. Li, B. Hu, W. Chen, W.-D. Liu, W. Lyu, J. MacLeod, Z.-G. Chen, *eScience* **2023**, *3*, 100122.
[13] M. H. Bagheri, A. A. Khan, S. Shahzadi, M. M. Rana, M. S. Hasan, D. Ban, *Nano Energy* **2024**, *120*, 109101.
[14] J. Liu, Y. He, L. Ding, H. Zhang, Q. Li, L. Jia, J. Yu, T. W. Lau, M. Li, Y. Qin, X. Gu, F. Zhang, Q. Li, Y. Yang, S. Zhao, X. Wu, J. Liu, T. Liu, Y. Gao, Y. Wang, X. Dong, H. Chen, P. Li, T. Zhou, M. Yang, X. Ru, F. Peng, S. Yin, M. Qu, D. Zhao, et al., *Nature* **2024**, *635*, 596.
[15] C. Zhou, Y. K. Lee, Y. Yu, S. Byun, Z.-Z. Luo, H. Lee, B. Ge, Y.-L. Lee, X. Chen, J. Y. Lee, O. Cojocaru-Mirédin, H. Chang, J. Im, S.-P. Cho, M. Wuttig, V. P. Dravid, M. G. Kanatzidis, I. Chung, *Nat. Mater.* **2021**, *20*, 1378.
[16] C. Chang, M. Wu, D. He, Y. Pei, C.-F. Wu, X. Wu, H. Yu, F. Zhu, K. Wang, Y. Chen, L. Huang, J.-F. Li, J. He, L.-D. Zhao, *Science* **2018**, *360*, 778.
[17] D.-Z. Wang, W.-D. Liu, M. Li, L.-C. Yin, H. Gao, Q. Sun, H. Wu, Y. Wang, X.-L. Shi, X. Yang, Q. Liu, Z.-G. Chen, *Chem. Eng. J.* **2022**, *441*, 136131.
[18] R. Liu, Z. L. Wang, K. Fukuda, T. Someya, *Nat. Rev. Mater.* **2022**, *7*, 870.
[19] Z. Wang, *MRS Bull.* **2023**, *48*, 1014.
[20] H. Guo, M.-H. Yeh, Y.-C. Lai, Y. Zi, C. Wu, Z. Wen, C. Hu, Z. L. Wang, *ACS Nano* **2016**, *10*, 10580.
[21] Y. Yang, L. Xie, Z. Wen, C. Chen, X. Chen, A. Wei, P. Cheng, X. Xie, X. Sun, *ACS Appl. Mater. Interfaces* **2018**, *10*, 42356.
[22] J. Han, C. Xu, J. Zhang, N. Xu, Y. Xiong, X. Cao, Y. Liang, L. Zheng, J. Sun, J. Zhai, Q. Sun, Z. L. Wang, *ACS Nano* **2021**, *15*, 1597.
[23] M. Liu, Z. Cong, X. Pu, W. Guo, T. Liu, M. Li, Y. Zhang, W. Hu, Z. L. Wang, *Adv. Funct. Mater.* **2019**, *29*, 1806298.
[24] K. Dong, Y.-C. Wang, J. Deng, Y. Dai, S. L. Zhang, H. Zou, B. Gu, B. Sun, Z. L. Wang, *ACS Nano* **2017**, *11*, 9490.
[25] X. Pu, L. Li, M. Liu, C. Jiang, C. Du, Z. Zhao, W. Hu, Z. L. Wang, *Adv. Mater.* **2016**, *28*, 98.
[26] Z. Cong, W. Guo, Z. Guo, Y. Chen, M. Liu, T. Hou, X. Pu, W. Hu, Z. L. Wang, *ACS Nano* **2020**, *14*, 5590.
[27] J. Han, N. Xu, J. Yu, Y. Wang, Y. Xiong, Y. Wei, Z. L. Wang, Q. Sun, *Energy Environ. Sci.* **2022**, *15*, 5069.
[28] W. Ma, M. Zhang, W. Yan, J. Zhu, J. Liu, W. Song, *Nano Energy* **2022**, *101*, 107601.
[29] B. K. Deka, A. Hazarika, M.-J. Kwak, D. C. Kim, A. P. Jaiswal, H. G. Lee, J. Seo, C. Jeong, J.-H. Jang, Y.-B. Park, H. W. Park, *Energy Storage Mater.* **2021**, *43*, 402.
[30] S. Qin, Q. Zhang, X. Yang, M. Liu, Q. Sun, Z. L. Wang, *Adv. Energy Mater.* **2018**, *8*, 1800069.
[31] M. Li, Y. Zhang, H. Wang, F. Wang, L. Liang, X. Wang, Y. Li, Y. Wu, X. Pu, H. Zheng, *Nano Energy* **2024**, *119*, 109073.
[32] A. Merchant, S. Batzner, S. S. Schoenholz, M. Aykol, G. Cheon, E. D. Cubuk, *Nature* **2023**, *624*, 80.
[33] Z. Wang, Z. Sun, H. Yin, H. Wei, Z. Peng, Y. X. Pang, G. Jia, H. Zhao, C. H. Pang, Z. Yin, *eScience* **2023**, *3*, 100136.
[34] C. Zhu, E. A. Bamidele, X. Shen, G. Zhu, B. Li, *Chem. Rev.* **2024**, *124*, 4258.
[35] W. L. Ng, G. L. Goh, G. D. Goh, J. S. J. Ten, W. Y. Yeong, *Adv. Mater.* **2024**, *36*, 2310006.
[36] N. G. An, J. Y. Kim, D. Vak, *Energy Environ. Sci.* **2021**, *14*, 3438.
[37] K. Kranthiraja, A. Saeki, *Adv. Funct. Mater.* **2021**, *31*, 2011168.
[38] Y. Hu, X. Hu, L. Zhang, T. Zheng, J. You, B. Jia, Y. Ma, X. Du, L. Zhang, J. Wang, B. Che, T. Chen, S. (Frank) Liu, *Adv. Energy Mater.* **2022**, *12*, 2201463.
[39] W. Yan, Y. Liu, Y. Zang, J. Cheng, Y. Wang, L. Chu, X. Tan, L. Liu, P. Zhou, W. Li, Z. Zhong, *Nano Energy* **2022**, *99*, 107394.
[40] V. C. Karade, S. S. Sutar, S. W. Shin, M. P. Suryawanshi, J. S. Jang, K. S. Gour, R. K. Kamat, J. H. Yun, T. D. Dongale, J. H. Kim, *Adv. Funct. Mater.* **2023**, *33*, 2303459.
[41] N. Meftahi, M. A. Surmiak, S. O. Fürer, K. J. Rietwyk, J. Lu, S. R. Raga, C. Evans, M. Michalska, H. Deng, D. P. McMeekin, T. Alan, D. Vak, A. S. R. Chesman, A. J. Christofferson, D. A. Winkler, U. Bach, S. P. Russo, *Adv. Energy Mater.* **2023**, *13*, 2203859.
[42] H. Wang, J. Feng, Z. Dong, L. Jin, M. Li, J. Yuan, Y. Li, *NPJ Comput. Mater.* **2023**, *9*, 1.
[43] X. Cai, F. Liu, A. Yu, J. Qin, M. Hatamvand, I. Ahmed, J. Luo, Y. Zhang, H. Zhang, Y. Zhan, *Light Sci. Appl.* **2022**, *11*, 234.
[44] Y. Zhu, D. W. Newbrook, P. Dai, C. H. K. de Groot, R. Huang, *Appl. Energy* **2022**, *305*, 117800.
[45] Y.-L. Lee, H. Lee, T. Kim, S. Byun, Y. K. Lee, S. Jang, I. Chung, H. Chang, J. Im, *J. Am. Chem. Soc.* **2022**, *144*, 13748.
[46] X. Jia, Y. Deng, X. Bao, H. Yao, S. Li, Z. Li, C. Chen, X. Wang, J. Mao, F. Cao, J. Sui, J. Wu, C. Wang, Q. Zhang, X. Liu, *NPJ Comput. Mater.* **2022**, *8*, 34.
[47] G. S. Na, H. Chang, *NPJ Comput. Mater.* **2022**, *8*, 214.
[48] M. Saeidi-Javash, K. Wang, M. Zeng, T. Luo, A. W. Dowling, Y. Zhang, *Energy Environ. Sci.* **2022**, *15*, 5093.

[49] C. Maduabuchi, C. Eneh, A. A. Alrobaian, M. Alkhedher, *Energy* **2023**, *263*, 125889.
[50] M. Li, H. Yuan, Y. Luo, X. Ma, H. Liu, W. Jiang, Y. Fang, *Adv. Energy Mater.* **2023**, *13*, 2300049.
[51] W. Demeke, B. Ryu, S. Ryu, *Appl. Energy* **2024**, *355*, 122216.
[52] R. Yuan, Z. Liu, P. V. Balachandran, D. Xue, Y. Zhou, X. Ding, J. Sun, D. Xue, T. Lookman, *Adv. Mater.* **2018**, *30*, 1702884.
[53] H. Jing, C. Guan, Y. Yang, H. Zhu, *J. Mater. Chem. A* **2023**, *11*, 14840.
[54] R. Yuan, Y. Tian, D. Xue, D. Xue, Y. Zhou, X. Ding, J. Sun, T. Lookman, *Adv. Sci.* **2019**, *6*, 1901395.
[55] W. Li, T. Yang, C. Liu, Y. Huang, C. Chen, H. Pan, G. Xie, H. Tai, Y. Jiang, Y. Wu, Z. Kang, L. Chen, Y. Su, Z. Hong, *Adv. Sci.* **2022**, *9*, 2105550.
[56] M. Khorsand, J. Tavakoli, H. Guan, Y. Tang, *Nano Energy* **2020**, *75*, 104993.
[57] Y. Wang, X. Liu, Z. Zheng, Y. Yin, X. Wang, Z. You, *Nano Energy* **2021**, *90*, 106570.
[58] M. Jiang, B. Li, W. Jia, Z. Zhu, *Nano Energy* **2022**, *93*, 106830.
[59] H. Zhou, F. Liu, J. Chen, J. Wang, Y. Wu, J. Chen, S. Chang, L. Xia, C. Zhang, J. Jiang, K. Dong, C. Zhang, L. Sun, W. Xuan, P. Zhao, H. Jin, S. Dong, J. Luo, *Nano Energy* **2023**, *118*, 108963.
[60] S. Varun, A. M. Chandran, K. P. Minhaj, V. Shaju, L. A. Varghese, P. K. S. Mural, *Chem. Eng. J.* **2024**, *484*, 149661.
[61] Z. L. Wang, A. C. Wang, *Mater. Today* **2019**, *30*, 34.
[62] S. Lin, X. Chen, Z. L. Wang, *Chem. Rev.* **2022**, *122*, 5209.
[63] C. Xu, Y. Zi, A. C. Wang, H. Zou, Y. Dai, X. He, P. Wang, Y.-C. Wang, P. Feng, D. Li, Z. L. Wang, *Adv. Mater.* **2018**, *30*, 1706790.
[64] Y. Li, Y. Luo, H. Deng, S. Shi, S. Tian, H. Wu, J. Tang, C. Zhang, X. Zhang, J.-W. Zha, S. Xiao, *Adv. Mater.* **2024**, *36*, 2314380.
[65] S. Fang, X. Ji, H. Wang, H. Jiang, M. Gao, H. Liu, Y. Liu, B. Cheng, *J. Mater. Chem. A* **2024**, *12*, 9322.
[66] M. Shanbedi, H. Ardebili, A. Karim, *Prog. Polym. Sci.* **2023**, *144*, 101723.
[67] X. Tao, X. Chen, Z. L. Wang, *Energy Environ. Sci.* **2023**, *16*, 3654.
[68] Y. Yu, H. Li, D. Zhao, Q. Gao, X. Li, J. Wang, Z. L. Wang, T. Cheng, *Mater. Today* **2023**, *64*, 61.
[69] P. Jiao, Z. L. Wang, A. H. Alavi, *Adv. Mater.* **2024**, *36*, 2308505.
[70] D. Liu, J. Zhang, S. Cui, L. Zhou, Y. Gao, Z. L. Wang, J. Wang, *Small Methods* **2023**, *7*, 2300562.
[71] W. Liu, Z. Wang, C. Hu, *Mater. Today* **2021**, *45*, 93.
[72] D. Tan, J. Zhou, K. Wang, C. Zhang, Z. Li, D. Xu, *Nano Energy* **2023**, *109*, 108315.
[73] X. Zhang, Y. Yu, X. Xia, W. Zhang, X. Cheng, H. Li, Z. L. Wang, T. Cheng, *Adv. Energy Mater.* **2023**, *13*, 2302353.
[74] Q. Mu, W. He, C. Shan, S. Fu, S. Du, J. Wang, Z. Wang, K. Li, C. Hu, *Adv. Funct. Mater.* **2024**, *34*, 2309421.
[75] J. Meng, L. Zhang, H. Liu, W. Sun, W. Wang, H. Wang, D. Yang, M. Feng, Y. Feng, D. Wang, *Adv. Energy Mater.* **2024**, *14*, 2303298.
[76] S. Yang, C. Zhang, Z. Du, Y. Tu, X. Dai, Y. Huang, J. Fan, Z. Hong, T. Jiang, Z. L. Wang, *Adv. Energy Mater.* **2024**, *14*, 2304184.
[77] Y. Yang, Q. Shi, Z. Zhang, X. Shan, B. Salam, C. Lee, *InfoMat* **2023**, *5*, 12360.
[78] G. Xu, X. Huang, R. Shi, Y. Yang, P. Wu, J. Zhou, X. He, J. Li, Y. Zen, Y. Jiao, B. Zhang, J. Li, G. Zhao, Y. Liu, Y. Huang, M. Wu, Q. Zhang, Z. Yang, X. Yu, *Adv. Funct. Mater.* **2024**, *34*, 2310777.
[79] F. Liu, Y. Feng, Y. Qi, G. Liu, H. Zhou, Y. Lin, B. Fan, Z. Zhang, S. Dong, C. Zhang, *InfoMat* **2023**, *5*, 12428.
[80] M. Kang, D.-M. Lee, I. Hyun, N. Rubab, S.-H. Kim, S.-W. Kim, *Chem. Rev.* **2023**, *123*, 11559.
[81] Y. Li, Z. Tian, X.-Z. Gao, H.-Y. Zhao, X. Li, Z. L. Wang, Z.-Z. Yu, D. Yang, *Adv. Funct. Mater.* **2023**, *33*, 2308845.
[82] I. Kim, H. Roh, J. Yu, N. Jayababu, D. Kim, *ACS Energy Lett.* **2020**, *5*, 1577.
[83] A. Chang, C. Uy, X. Xiao, X. Xiao, J. Chen, *Nano Energy* **2022**, *98*, 107282.
[84] M. Zhang, J. Li, L. Kang, N. Zhang, C. Huang, Y. He, M. Hu, X. Zhou, J. Zhang, *Nanoscale* **2020**, *12*, 3988.
[85] Y. Hu, M. Wu, M. Yuan, Y. Wen, P. Ren, S. Ye, F. Liu, B. Zhou, H. Fang, R. Wang, Z. Ji, R. Huang, *Appl. Phys. Lett.* **2024**, *125*, 152905.
[86] Q. Wang, X. Wang, X. Zhang, S. Li, T. Wang, *Tribol. Int.* **2023**, *188*, 108815.
[87] Y. Zi, S. Niu, J. Wang, Z. Wen, W. Tang, Z. L. Wang, *Nat. Commun.* **2015**, *6*, 8376.
[88] J. Shao, T. Jiang, W. Tang, X. Chen, L. Xu, Z. L. Wang, *Nano Energy* **2018**, *51*, 688.
[89] Y. Liu, W. Liu, Z. Wang, W. He, Q. Tang, Y. Xi, X. Wang, H. Guo, C. Hu, *Nat. Commun.* **2020**, *11*, 1599.
[90] H. Zou, Y. Zhang, L. Guo, P. Wang, X. He, G. Dai, H. Zheng, C. Chen, A. C. Wang, C. Xu, Z. L. Wang, *Nat. Commun.* **2019**, *10*, 1427.
[91] H. Zou, L. Guo, H. Xue, Y. Zhang, X. Shen, X. Liu, P. Wang, X. He, G. Dai, P. Jiang, H. Zheng, B. Zhang, C. Xu, Z. L. Wang, *Nat. Commun.* **2020**, *11*, 2093.
[92] J. Wang, C. Wu, Y. Dai, Z. Zhao, A. Wang, T. Zhang, Z. L. Wang, *Nat. Commun.* **2017**, *8*, 88.
[93] Y. Li, Z. Zhao, L. Liu, L. Zhou, D. Liu, S. Li, S. Chen, Y. Dai, J. Wang, Z. L. Wang, *Adv. Energy Mater.* **2021**, *11*, 2100050.
[94] R. L. Bulathsinghala, A. Ravichandran, H. Zhao, W. Ding, R. D. I. G. Dharmasena, *Nano Energy* **2024**, *123*, 109383.
[95] S.-J. Park, M.-L. Seol, D. Kim, S.-B. Jeon, Y.-K. Choi, *Nano Energy* **2016**, *21*, 258.
[96] W. Yang, X. Wang, H. Li, J. Wu, Y. Hu, Z. Li, H. Liu, *Nano Energy* **2019**, *57*, 41.
[97] J. Huang, X. Fu, G. Liu, S. Xu, X. Li, C. Zhang, L. Jiang, *Nano Energy* **2019**, *62*, 638.
[98] S. Mishra, P. Supraja, D. Haranath, R. R. Kumar, S. Pola, *Nano Energy* **2022**, *104*, 107964.
[99] S.-H. Shin, Y. H. Kwon, Y.-H. Kim, J.-Y. Jung, M. H. Lee, J. Nah, *ACS Nano* **2015**, *9*, 4621.
[100] S.-H. Shin, Y. E. Bae, H. K. Moon, J. Kim, S.-H. Choi, Y. Kim, H. J. Yoon, M. H. Lee, J. Nah, *ACS Nano* **2017**, *11*, 6131.
[101] M. P. Kim, Y. Lee, Y. H. Hur, J. Park, J. Kim, Y. Lee, C. W. Ahn, S. W. Song, Y. S. Jung, H. Ko, *Nano Energy* **2018**, *53*, 37.
[102] S. Li, J. Nie, Y. Shi, X. Tao, F. Wang, J. Tian, S. Lin, X. Chen, Z. L. Wang, *Adv. Mater.* **2020**, *32*, 2001307.
[103] Y. Liu, C. Zhang, B. Zhang, W. Yuan, O. Yang, Y. Hu, L. Zhou, Z. Zhao, J. Xiao, Z. L. Wang, J. Wang, *J. Mater. Chem. A* **2022**, *10*, 16547.
[104] J. Kim, H. Ryu, J. H. Lee, U. Khan, S. S. Kwak, H.-J. Yoon, S.-W. Kim, *Adv. Energy Mater.* **2020**, *10*, 1903524.
[105] X. Tao, S. Li, Y. Shi, X. Wang, J. Tian, Z. Liu, P. Yang, X. Chen, Z. L. Wang, *Adv. Funct. Mater.* **2021**, *31*, 2106082.
[106] L. Liu, J. Li, W. Ou-Yang, Z. Guan, X. Hu, M. Xie, Z. Tian, *Nano Energy* **2022**, *96*, 107139.
[107] J. Sun, H. Choi, S. Cha, D. Ahn, M. Choi, S. Park, Y. Cho, J. Lee, T. Park, J.-J. Park, *Adv. Funct. Mater.* **2022**, *32*, 2109139.
[108] H. Wu, S. Fu, W. He, C. Shan, J. Wang, Y. Du, S. Du, B. Li, C. Hu, *Adv. Funct. Mater.* **2022**, *32*, 2203884.
[109] Q. Zhao, H. Wu, J. Wang, S. Xu, W. He, C. Shan, S. Fu, G. Li, K. Li, C. Hu, *Adv. Energy Mater.* **2023**, *13*, 2302099.
[110] X. Wen, Y. Su, Y. Yang, H. Zhang, Z. L. Wang, *Nano Energy* **2014**, *4*, 150.
[111] C. X. Lu, C. B. Han, G. Q. Gu, J. Chen, Z. W. Yang, T. Jiang, C. He, Z. L. Wang, *Adv. Eng. Mater.* **2017**, *19*, 1700275.
[112] V. Nguyen, R. Yang, *Nano Energy* **2013**, *2*, 604.
[113] K. Wang, Z. Qiu, J. Wang, Y. Liu, R. Chen, H. An, J. H. Park, C. H. Suk, C. Wu, J. Lin, T. W. Kim, *Nano Energy* **2022**, *93*, 106880.
[114] D. Liu, L. Zhou, S. Cui, Y. Gao, S. Li, Z. Zhao, Z. Yi, H. Zou, Y. Fan, J. Wang, Z. L. Wang, *Nat. Commun.* **2022**, *13*, 6019.
[115] S. Niu, S. Wang, L. Lin, Y. Liu, Y. S. Zhou, Y. Hu, Z. L. Wang, *Energy Environ. Sci.* **2013**, *6*, 3576.

[116] H. Zhang, C. Zhang, J. Zhang, L. Quan, H. Huang, J. Jiang, S. Dong, J. Luo, *Nano Energy* **2019**, *61*, 442.
[117] S. Niu, Y. Liu, X. Chen, S. Wang, Y. S. Zhou, L. Lin, Y. Xie, Z. L. Wang, *Nano Energy* **2015**, *12*, 760.
[118] S. Niu, Y. Liu, S. Wang, L. Lin, Y. S. Zhou, Y. Hu, Z. L. Wang, *Adv. Funct. Mater.* **2014**, *24*, 3332.
[119] Z. Chen, K. Dai, J. Chen, J. Zhuo, D. Zhao, R. Ma, X. Zhang, X. Li, X. Wang, G. Yang, F. Yi, *Adv. Sci.* **2023**, *10*, 2206950.
[120] H. Zhang, L. Quan, J. Chen, C. Xu, C. Zhang, S. Dong, C. Lü, J. Luo, *Nano Energy* **2019**, *56*, 700.
[121] S. Niu, Y. Liu, S. Wang, L. Lin, Y. S. Zhou, Y. Hu, Z. L. Wang, *Adv. Mater.* **2013**, *25*, 6184.
[122] J. Shao, T. Jiang, W. Tang, L. Xu, T. W. Kim, C. Wu, X. Chen, B. Chen, T. Xiao, Y. Bai, Z. L. Wang, *Nano Energy* **2018**, *48*, 292.
[123] A. Jain, S. P. Ong, G. Hautier, W. Chen, W. D. Richards, S. Dacek, S. Cholia, D. Gunter, D. Skinner, G. Ceder, K. A. Persson, *APL Mater.* **2013**, *1*, 011002.
[124] A. Belsky, M. Hellenbrandt, V. L. Karen, P. Luksch, *Acta Cryst. B* **2002**, *58*, 364.
[125] S. Gražulis, D. Chateigner, R. T. Downs, A. F. T. Yokochi, M. Quirós, L. Lutterotti, E. Manakova, J. Butkus, P. Moeck, A. Le Bail, *J. Appl. Cryst.* **2009**, *42*, 726.
[126] L. M. Ghiringhelli, J. Vybiral, S. V. Levchenko, C. Draxl, M. Scheffler, *Phys. Rev. Lett.* **2015**, *114*, 105503.
[127] M. Greenacre, P. J. F. Groenen, T. Hastie, A. I. D'Enza, A. Markos, E. Tuzhilina, *Nat. Rev. Methods Primers* **2022**, *2*, 100.
[128] L. van der Maaten, G. Hinton, *J. Mach. Learn. Res.* **2008**, *9*, 2579.
[129] D. H. Wolpert, W. G. Macready, *IEEE Trans. Evol. Computat.* **1997**, *1*, 67.
[130] P. Probst, A.-L. Boulesteix, B. Bischl, *J. Mach. Learn. Res.* **2019**, *20*, 1.
[131] S. Amari, *Neurocomputing* **1993**, *5*, 185.
[132] W.-Y. Jin, M. M. Ovhal, H. B. Lee, B. Tyagi, J.-W. Kang, *Adv. Energy Mater.* **2021**, *11*, 2003509.
[133] J. Lee, F. Shen, S. Miao, G. H. Ryu, B. Im, D. G. Kim, G.-H. An, Y. Cho, *Nano Energy* **2022**, *104*, 107891.
[134] W. He, X. Fu, D. Zhang, Q. Zhang, K. Zhuo, Z. Yuan, R. Ma, *Nano Energy* **2021**, *84*, 105880.
[135] R. Yuan, Y. Dong, R. Hou, S. Zhang, H. Song, *J. Electrochem. Soc.* **2022**, *169*, 030504.
[136] H. Yang, Z. He, M. Zhang, X. Tan, K. Sun, H. Liu, N. Wang, L. Guan, C. Wang, Y. Wan, W. Wang, H. Hu, M. Wu, *EcoMat* **2023**, *5*, 12330.
[137] W. Sha, Y. Li, S. Tang, J. Tian, Y. Zhao, Y. Guo, W. Zhang, X. Zhang, S. Lu, Y.-C. Cao, S. Cheng, *InfoMat* **2021**, *3*, 353.
[138] C. Lv, X. Zhou, L. Zhong, C. Yan, M. Srinivasan, Z. W. Seh, C. Liu, H. Pan, S. Li, Y. Wen, Q. Yan, *Adv. Mater.* **2022**, *34*, 2101474.
[139] C. Li, K. Zheng, *InfoMat* **2023**, *5*, 12425.
[140] S. Jha, M. Yen, Y. S. Salinas, E. Palmer, J. Villafuerte, H. Liang, *J. Mater. Chem. A* **2023**, *11*, 3904.
[141] T. Zhou, Z. Song, K. Sundmacher, *Engineering* **2019**, *5*, 1017.
[142] K. L. Van Aken, M. Beidaghi, Y. Gogotsi, *Angew. Chem., Int. Ed.* **2015**, *54*, 4806.
[143] W. Tian, D. Cheng, S. Wang, C. Xiong, Q. Yang, *Appl. Surf. Sci.* **2019**, *495*, 143589.
[144] S. Fan, L. Wei, X. Liu, W. Ma, C. Lou, J. Wang, Y. Zhang, *Int. J. Hydrogen Energy* **2021**, *46*, 39969.
[145] M. Xia, J. Nie, Z. Zhang, X. Lu, Z. L. Wang, *Nano Energy* **2018**, *47*, 43.
[146] T. Tevi, A. Takshi, *J. Power Sources* **2015**, *273*, 857.
[147] Y. Zhang, L. Wei, X. Liu, W. Ma, C. Lou, J. Wang, S. Fan, *J. Power Sources* **2022**, *543*, 231851.
[148] W. Zheng, L. Yang, P. Zhang, V. Natu, Z. Sun, J. Rosen, M. W. Barsoum, *Energy Storage Mater.* **2023**, *63*, 103037.
[149] P. Liu, Y. Wen, L. Huang, X. Zhu, R. Wu, S. Ai, T. Xue, Y. Ge, *J. Electroanal. Chem.* **2021**, *899*, 115684.
[150] R. Kushwaha, M. K. Singh, S. Krishnan, D. K. Rai, *J. Mater. Sci.* **2023**, *58*, 15448.
[151] T. Wang, R. Pan, M. L. Martins, J. Cui, Z. Huang, B. P. Thapaliya, C.-L. Do-Thanh, M. Zhou, J. Fan, Z. Yang, M. Chi, T. Kobayashi, J. Wu, E. Mamontov, S. Dai, *Nat. Commun.* **2023**, *14*, 4607.
[152] M. Zhou, A. Vassallo, J. Wu, *ACS Appl. Energy Mater.* **2020**, *3*, 5993.
[153] S. Zhu, J. Li, L. Ma, C. He, E. Liu, F. He, C. Shi, N. Zhao, *Mater. Lett.* **2018**, *233*, 294.
[154] H. Su, S. Lin, S. Deng, C. Lian, Y. Shang, H. Liu, *Nanoscale Adv.* **2019**, *1*, 2162.
[155] S. Mishra, R. Srivastava, A. Muhammad, A. Amit, E. Chiavazzo, M. Fasano, P. Asinari, *Sci. Rep.* **2023**, *13*, 6494.
[156] A. G. Saad, A. Emad-Eldeen, W. Z. Tawfik, A. G. El-Deen, *J. Energy Storage* **2022**, *55*, 105411.
[157] W. G. Buxton, S. G. King, V. Stolojan, *Energy Environ. Mater.* **2023**, *6*, 12363.
[158] K. Liu, C. Yu, W. Guo, L. Ni, J. Yu, Y. Xie, Z. Wang, Y. Ren, J. Qiu, *J. Energy Chem.* **2021**, *58*, 94.
[159] J. Wang, B. Ding, X. Hao, Y. Xu, Y. Wang, L. Shen, H. Dou, X. Zhang, *Carbon* **2016**, *102*, 255.
[160] H. Pourkheirollah, J. Keskinen, M. Mäntysalo, D. Lupo, *J. Power Sources* **2023**, *567*, 232932.
[161] R. Kunwar, B. Pal, I. Izwan Misnon, H. Daniyal, F. Zabihi, S. Yang, Z. Sofer, C.-C. Yang, R. Jose, *Appl. Energy* **2023**, *334*, 120658.
[162] M. Kaus, J. Kowal, D. U. Sauer, *Electrochim. Acta* **2010**, *55*, 7516.
[163] T. Ghanbari, E. Moshksar, S. Hamedi, F. Rezaei, Z. Hosseini, *J. Power Sources* **2021**, *495*, 229787.
[164] J. Kowal, E. Avaroglu, F. Chamekh, A. Šenfelds, T. Thien, D. Wijaya, D. U. Sauer, *J. Power Sources* **2011**, *196*, 573.
[165] W. Li, M. Wu, W. Yang, M. Zhao, X. Lu, *Electrochim. Acta* **2023**, *438*, 141550.
[166] K. Wang, L. Yao, M. Jahon, J. Liu, M. Gonzalez, P. Liu, V. Leung, X. Zhang, T. N. Ng, *ACS Energy Lett.* **2020**, *5*, 3276.
[167] P. T. Nguyen, J. Jang, Y. Lee, S. T. Choi, J. B. In, *J. Mater. Chem. A* **2021**, *9*, 4841.
[168] H. Sun, S. Xie, Y. Li, Y. Jiang, X. Sun, B. Wang, H. Peng, *Adv. Mater.* **2016**, *28*, 8431.
[169] W. Kang, L. Zeng, S. Ling, C. Zhang, *Adv. Energy Mater.* **2021**, *11*, 2100020.
[170] A. Marcato, J. E. Santos, C. Liu, G. Boccardo, D. Marchisio, A. A. Franco, *Energy Storage Mater.* **2023**, *63*, 102927.
[171] X. Liu, D. Ji, X. Jin, V. Quintano, R. Joshi, *Carbon* **2023**, *214*, 118342.

Rui Gu received his bachelor's degree from the University of Science and Technology Beijing in 2020. He is now a Ph.D. candidate at the Beijing Institute of Nanoenergy and Nanosystems, Chinese Academy of Sciences. His research interests focus on energy harvesting and sensing devices based on triboelectric nanogenerators.

Liang Wei obtained his master's degree from Qiqihar University in 2022 and is currently a doctoral student jointly at Guangxi University and the Beijing Institute of Nanoenergy and Nanosystems (BINN), Chinese Academy of Sciences. His research interests focus on TENG-based self-powered systems and graphene-based supercapacitors.

Nuo Xu received her B.S. degree from South China University in 2017. She is now a PhD student at the School of Physical Science and Engineering Technology, Guangxi University, where she is co-trained at the Institute of Nanoenergy and Nanosystems, Beijing, under the supervision of Prof. Qijun Sun. Her research focuses on the study of paper-based electronic circuits and their neuromorphic devices.

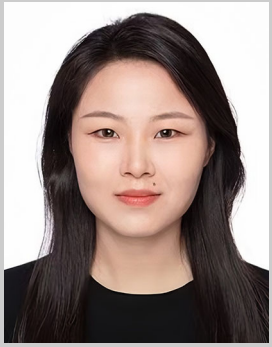

Yao Xiong received her Ph.D. from the University of Chinese Academy of Sciences in 2024. Now she is a postdoc in the Beijing Institute of Nanoenergy and Nanosystems, Chinese Academy of Sciences. Her research direction mainly includes energy harvesting, self-powered sensors, and corresponding intelligent application.

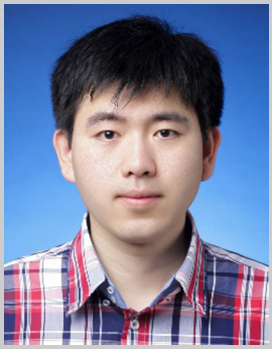

Qijun Sun joined the Beijing Institute of Nanoenergy and Nanosystems (CAS) in 2016, as the principal investigator of Functional Soft Electronics Lab. The main research interests of his group include triboiontronic devices, mechanoplastic neuromorphic transistors, artificial synaptic devices electronic skin, 2D materials-based flexible semiconductor devices, human-machine interactive systems, and micro-nano fabrication, aiming to develop advanced systems for human health monitoring and human-robotic interface.

Zhong Lin Wang received his Ph. D from Arizona State University in physics. He now is the Hightower Chair in Materials Science and Engineering, Regents' Professor, Engineering Distinguished Professor, and Director, the Center for Nanostructure Characterization, at Georgia Tech. Dr. Wang has made original and innovative contributions to the synthesis, discovery, characterization, and understanding of fundamental physical properties of oxide nanobelts and nanowires, as well as applications of nanowires in energy sciences, electronics, optoelectronics, and biological science. He pioneered the field of piezotronics and piezo-phototronics by introducing piezoelectric potential gated charge transport process in fabricating new electronic and optoelectronic devices.